

Article

Evaluation of CMORPH, PERSIANN-CDR, CHIRPS V2.0, TMPA 3B42 V7, and GPM IMERG V6 Satellite Precipitation Datasets in Arabian Arid Regions

Ahmed M. Helmi ^{1,*} and Mohamed S. Abdelhamed ^{1,2,3}¹ Irrigation and Hydraulics Department, Faculty of Engineering, Cairo University, Cairo 12613, Egypt² Global Institute for Water Security, University of Saskatchewan, Saskatoon, SK S7N 3H5, Canada³ Department of Civil and Geological Engineering, University of Saskatchewan, Saskatoon, SK S7N 5A9, Canada

* Correspondence: ahmed.helmi@eng.cu.edu.eg

Abstract: Rainfall depth is a crucial parameter in water resources and hydrological studies. Rain gauges provide the most reliable point-based rainfall estimates. However, they do not have a proper density/distribution to provide sufficient rainfall measurements in many areas, especially in arid regions. To evaluate the adequacy of satellite datasets as an alternative to the rain gauges, the Kingdom of Saudi Arabia (KSA) is selected for the current study as a representative of the arid regions. KSA occupies most of the Arabian Peninsula and is characterized by high variability in topographic and climatic conditions. Five satellite precipitation datasets (SPDSs)—CMORPH, PERSIANN-CDR, CHIRPS V2.0, TMPA 3B42 V7, and GPM IMERG V6—are evaluated versus 324 conventional rain-gauges' daily precipitation measures. The evaluation is conducted based on nine quantitative and categorical metrics. The evaluation analysis is carried out for daily, monthly, yearly, and maximum yearly records. The daily analysis revealed a low correlation for all SPDSs (<0.31), slightly improved in the yearly and maximum yearly analysis and reached its highest value (0.58) in the monthly analysis. The GPM IMERG V6 and PERSIANN-CDR have the highest probability of detection (0.55) but with a high false alarm ratio (>0.8). Accordingly, in arid regions, the use of daily SPDSs in rainfall estimation will lead to high uncertainty in the obtained results. The best performance for all statistical metrics was found at 500–750 m altitudes in the central and northern parts of the study area for all satellites except minor anomalies. CMORPH dataset has the lowest centered root mean square error (RMSEc) for all analysis periods with the best results in the monthly analyses.

Keywords: CMORPH; PERSIANN-CDR; CHIRPS V2.0; TMPA 3B42 V7; GPM IMERG V6; satellite precipitation data; NSE; KGE; Arabian arid regions; hydrology

Citation: Helmi, A.M.; Abdelhamed, M.S. Evaluation of CMORPH, PERSIANN-CDR, CHIRPS V2.0, TMPA 3B42 V7, and GPM IMERG V6 Satellite Precipitation Datasets in Arabian Arid Regions. *2023*, *15*, 92. <https://doi.org/10.3390/w15010092>

Academic Editors: David Pulido-Velázquez, Antonio Juan Collados-Lara and Simon Stisen

Received: 10 November 2022

Revised: 23 December 2022

Accepted: 23 December 2022

Published: 27 December 2022



Copyright: © 2022 by the authors. Licensee MDPI, Basel, Switzerland. This article is an open access article distributed under the terms and conditions of the Creative Commons Attribution (CC BY) license (<https://creativecommons.org/licenses/by/4.0/>).

1. Introduction

Precipitation is a major driving component in the hydrological cycle [1]. Accurate measurements and reliable forecasting of rainfall characteristics significantly influence the reliability of the hydrological and water resources modeling [2]. Rain gauges' measurements are the most reliable source for rainfall characterization [3–5]. To achieve sufficient spatiotemporal rainfall distribution, rain gauges should be properly distributed over the entire study area. However, the existing rain gauges are sparsely distributed in many countries due to climatic, topographic complexity, and even internal conflicts [6–8]. The currently available satellite-based precipitation datasets (SPDSs) have a quasi-global coverage with different spatial resolutions and temporal coverages. The SPDSs temporal resolutions start from 30 min and spatial resolutions start from 0.0375° . The temporal coverage starts from 1981 to the near present. Further, SPDSs can be incorporated to address

the insufficient spatial coverage of rain gauges [9]. Table 1 summarizes the characteristics of some available SPDSs.

Table 1. Characteristics of some available precipitation datasets.

Precipitation Product	Spatial Coverage				Temporal Coverage		Maximum Spatial Resolution	Maximum Temporal Resolution	Reference
	West	East	South	North	From	To			
The African rainfall climatology–V2 (ARC)	20°	55°	40°	40°	1983	Near Present	0.1° × 0.1°	10 Days	[10]
Tropical applications of meteorology using satellite data and ground-based observations (TAMSAT)	20°	55°	40°	40°	1983	Near Present	0.0375° × 0.0375°	Daily	[11]
Global precipitation climatology center (GPCP)	180°	180°	90°	90°	2000	2020	0.5° × 0.5°	Daily	[12]
Climate prediction center (CPC)	180°	180°	89.5°	89.5°	1979	Near Present	0.5° × 0.5°	Daily	[13]
Tropical rainfall measuring mission–3B43 V7 (TRMM)	180°	180°	50°	50°	1998	2019	0.25° × 0.25°	3 h	[14]
Climate prediction center morphing method (CMORPH)	180°	180°	60°	60°	1998	Near Present	8 × 8 km	30 min	[15]
Precipitation estimation from remotely sensed information using artificial neural networks (PERSIANN)	180°	180°	60°	60°	2000	Near Present	0.25° × 0.25°	1 h	[16]
PERSIANN-climate data record (PERSIANN-CDR)	180°	180°	60°	60°	1983	Near Present	0.25° × 0.25°	Daily	[17]
PERSIANN–cloud classification system (PERSIANN-CCS)	180°	180°	60°	60°	2003	Near Present	0.04° × 0.04°	1 h	[18]
Climate hazards group infrared Precipitation combined with terrestrial stations observations (CHIRPS)	180°	180°	50°	50°	1981	Near Present	0.05° × 0.05°	Daily	[19]
The global precipitation measurement mission (GPM)	180°	180°	90°	90°	2000	Near Present	0.1° × 0.1°	30 min	[20]

The accuracy of SPDSs has been extensively studied in many regions over the globe, following two approaches: (1) utilizing the satellite rainfall data in large-scale hydrological models and comparing the simulated hydrographs with recorded ones, or (2) comparing SPDSs values against the corresponding rain-gauge measurements.

The first approach was applied in the assessment of seventeen precipitation products' usage adequacy in modeling the stream flow for the Volta River basin (VRB: 415,600 km² drainage area) in West Africa for the 2009–2012 period. TAMSAT, CHIRPS, and PERSIANN-CDR were found to be the best-performing precipitation datasets based on daily streamflow evaluation [21]. TMPA 3B42 V7 precipitation dataset was utilized in the hydrologic modeling of the Gandak Himalayan River (44,797 km² drainage area) using the soil water assessment (SWAT) model [22]. The rainfall was evaluated for a 10 year period (2000–2010). The results showed that the use of TRMM data is suitable for moderate (7.5–35.4 mm/day) and heavy (35.5–124.4 mm/day) rainfall intensities and did not perform well for light (<7.5 mm/day) and extra-heavy (>124.4 mm/day) rainfall intensities. A summary of some previous SPDSs hydrological modeling studies is given in Table 2.

Table 2. Review of previous SPDSs hydrological modeling studies.

SPDSs	Region	Duration	Main Conclusions	Reference
TMPA-3B42V6	Tapajos river, 500,000 km ² , Brazil.	2000–2003	The generated modeled hydrographs had acceptable accuracy based on the comparison with 23 flow gauges along the river and its tributaries.	[23]
CMORPH TMPA-3B42RT TMPA 3B42 PERSIANN	Gilgel Abay, 1656 km ² , a mountainous watershed in northwest Ethiopia	2006–2007	The microwave-based SPDSs (CMORPH and TMPA 3B42RT) had a better performance than the infrared-based dataset (PERSIANN). The merged rain gauges and satellite data (TMPA 3B42) gave to lowest performance and inconsistencies	[24]
TMPA-3B42V7 CHIRPS, CFSR PERSIANN-CDR	Lake Ziway basin, 7311 km ² , Ethiopia	1985–2004	All SPDSs have a low correlation on daily temporal scale runoff simulations. CHIRPS, PERSIANN-CDR, and TRMM had good performance on the monthly temporal scale.	[25]
CHIRPS, CMORPH TMPA-3B42 V7 PERSIANN	Ganjiang River Basin, 80,948 km ² , China	2000–2014	TMPA outperformed other SPDSs. CMORPH PDS significantly underestimated streamflow.	[26]
CHIRPS, PERSIANN-CCS, IMERG	West Rapti River basin, 5082 km ² , Western Nepal	1986–2015	The IMERG SPDS had the best accuracy among the used SPDSs.	[27]
TMPA-3B42V7 CHIRPS	Eastern Nile Basin, 325,000 km ² , East Africa	1998–2007	TMPA 3B42V7 slightly had a better performance than CHIRPS in calculating the modeled monthly stream flow.	[28]
CHIRPS, PERSIANN-CDR TMPA 3B42 V7	Three different climate basins in China	2002–2015	The three SPDSs performed better in humid regions than in arid ones. TMPA 3B42 V7 showed the best performance over CHIRPS and PERSIANN-CDR, respectively. PERSIANN-CDR had the best performance in the arid basin. Low accuracy included for the three SPDSs on a daily scale	[29]

The second approach was applied in the assessment of TMPA, PERSIANN, CMORPH, and GMap SPDSs in nine mountainous regions around the globe [30] (the Blue Nile in Eastern Africa, the Himalayas in Nepal, the Alps in Italy and Switzerland, French Cevennes, the Andes in Peru and Columbia, the Rocky Mountains in U.S., and Taiwan). A minimum of 6 years of temporal coverage for each region was considered. Many SPDSs underestimated the rainfall depth in the wet season and, on the contrary, overestimated the dry season depth. The performance of the SPDSs was highly affected by seasonality. Furthermore, the accuracy of GMap, IMERG, and CHIRPS to produce rainfall estimates over Bali Island versus 27 rain-gauge records from 2015 to 2017 was evaluated [31]. The study was performed for different temporal scales (i.e., daily, pentadal, monthly, and annual). The GPM SPDS outperformed other SPDSs in all temporal resolutions and different altitudes.

SPDS data were also used to generate the temporal and spatial distribution of rainfall over large catchments characterized by a sparsely distributed network. Egypt, one of the most hyper-arid lands in the world, is an example of this regard [32]. The generated data for Egypt were used in simulating the hydrologic response of Wadi El Arish in Sinai with a catchment area of 23,000 km² [33] and a 176 km² subbasin of wadi Qena in the Egyptian Eastern Desert [34]. A summary of some previous studies that compared the SPDS-based rainfall to conventional rain gauges for evaluating the SPDSs accuracy is provided in Table 3.

Table 3. Review of SPDSs assessment studies based on rain gauges' measurements comparison.

SPDSs	Region	Ground Stations	Temporal Resolution	Duration	Main Conclusions	Reference
TMPA-3B42	IRAN	Grid *	Annual	1998–2006	The TRMM precipitation dataset underestimated the average annual precipitation.	[35]
PERSIANN-CDR	China	1400	Daily Extreme Events	1983–2006	PERSIANN-CDR efficiently captured the precipitation behavior, especially in humid areas. The efficiency was significantly reduced in arid and mountainous areas.	[36]
TMPA-3B42	Iraq	4	Monthly	2000–2010	Acceptable agreement between TMPA3B42 and ground stations for monthly temporal scale.	[37]
TMPA-3B42V7, PERSIANN, CMORPH	Iran	1000	Daily	2003–2008	3B42V7 had a better performance than the SPDSs.	[38]
IMERG V6, TMPA-3B42 V7 GSMaP	India	Grid **	Daily	Single monsoon 2014	The IMERG and GSMaP SPDSs showed better performance than TMPA SPDS, especially for low precipitation rates.	[39]
CHIRPS	China	2480	Daily	1981–2014	CHIRPS performed better for large rainfall depths than it does in arid and semi-arid land. The variation of CHIRPS performance is strongly affected by monsoon movement.	[40]
GPM-IMERG (early, late, final)	KSA	189	Daily	October 2015 April 2016	IMERG's final run showed significant improvement over the early and late run over 80% of the KSA area.	[41]
TMPA-3B42V7, CMORPH GPM-IMERGV05	China	542	Daily Seasonal Annual	2014–2017	IMERG results had better performance than TMPA 3B42 and CMORPH SPDSs. The quality of precipitation estimates reduced over the Tibetan plateau.	[42]
GPM IMERG (03,04, 05)	CHINA	30,000	Daily	June 2014 May 2015	V04 and V05 Final run show significant differences and improvements from V03 except for mountainous and arid zones.	[43]
PERSIANN-CDR PERSIANN TMPA-3B42 CMORPH	KSA	29	Daily Monthly	2003–2011	All satellites performed better in the wet season.	[44]
GSMaP GPM-IMERG CHIRPS	Egypt	29	Daily	March 2014 May 2018	None of the SPDSs showed consistent performance to be evaluated as the best quality or lowest quality among them.	[45]
TMPA-3B42 GPM-IMERG	CHINA	830	Daily	2000–2017	The GPM dataset outperformed the TRMM dataset over the same. The performance is better in humid areas and reduced in arid and mountainous areas.	[46]
TMPA 3B43V7	India	Grid **	Monthly	1998–2013	The correlation is higher during post-monsoon and winter seasons than pre-monsoon and monsoon seasons.	[47]
CMORPH-CRT	Mexico	14	30 min and Daily	2000–2018	Weak to moderate correlation with ground stations. CMORPH-CRT overestimates the number of rainy days.	[48]
CMORPH	South Africa	60	Daily, Weekly, Seasonal	1998–2013	CMORPH predicts 60% of rainfall events. The performance in lower temporal resolution (weeks or months) is better than in high temporal resolution (days).	[49]
GPM IMERG V6 TMPA 3B42V7	CHINA	13	Daily	2009–2017	The GPM dataset performed better than the TRMM dataset. The correlation coefficient for both falls below 0.6.	[50]
CHIRPS	BRAZIL	45	Monthly, Annual	1981–2017	CHIRPS dataset has a good correlation with mean monthly data with underestimation for the rainiest months and extreme rainfall events. It was concluded that the CHIRPS data could not provide a proper presentation of the trends in rainfall indices.	[51]
16 SPDSs	Nigeria	11	Monthly	2000–2012	The IMERG SPDS is consistent with its predecessor TMPA, and the best performance was concluded for IMERG-V6 and Multi-Source Weighted-Ensemble Precipitation MSWEP v. 2.2.	[52]
CMORPH	South Korea	48	Hourly, Daily, Monthly, Annual	1998–2015	CMORPH underestimates precipitation over South Korea. Annual-to-daily resolution can be used adequately in hydrological modeling. The hourly resolution requires corrections.	[53]
CHIRPS	Ethiopia	6	Monthly	1991–2015	CHIRPS overestimates the mean monthly data but with a strong positive linear correlation.	[54]

TMPA 3B42V7 CMORPH	Thailand	120	Daily, Monthly, and Annual	1998–2012	Both TRMM and CMORPH had limited ability for producing the characteristics of extreme events. Generally, the TRMM outperformed the CMORPH in representing precipitation.	[55]
TMPA-3B42V7, CMORPH IMERGV05	Tibetan Plateau China	87	Monthly An- nual	2001–2016	GPM outperformed the TRMM and CMORPH. Under-estimation of the annual precipitation was recorded for the three satellites.	[56]
PERSIANN-CCS, PERSIANN-CDR SM2RAIN-ASCAT CHIRPS-2.0	Punjab Province— Pakistan	26	Daily, Monthly, Seasonal An- nual	2010–2018	CHIRPS-2.0 and SM2RAIN-ASCAT outperformed PERSIANN products.	[57]

Note(s): * Iran synoptic gauges' data of the Islamic Republic of Iran Meteorological Organization (IRIMO) Version 0902, $0.25^\circ \times 0.25^\circ$ gridded precipitation [35]. ** India Meteorological Department (IMD) $0.25^\circ \times 0.25^\circ$ gridded precipitation [58].

Based on the abovementioned studies, it can be concluded that the accuracy of SPDSs in capturing the spatiotemporal characteristics of rainfall depth has a significant variability. The variability is affected by the intensity of rainfall, altitude, and geographic locations. The efficiency of SPDSs improved in coarser temporal resolution since many studies concluded significant accuracy improvement in monthly and annual temporal resolution over the daily ones. However, few studies evaluated the efficiency of SPDSs in arid and semi-arid regions, such as the Arabian Peninsula. The Kingdom of Saudi Arabia (KSA) constitutes most of the Arabian Peninsula area, with relatively dense rain gauges in some areas and sparse in others. The topography of KSA has a wide variability from low flat terrains in coastal areas, mountainous terrain, and flat plateaus [59]. The available rain-gauges in the KSA provide a long record of total daily precipitation. Our goals in the current study are to:

- Assess the accuracy of PERSIANN-CDR, CMORPH, CHIRPS V2.0, TMPA 3B42 V7, and GPM IMERG V6 Final Run to capture the precipitation characteristics versus rain gauges' measurements at different temporal resolutions in arid zones.
- Evaluate the SPDSs performance at different altitudes.

Additionally, we utilized a larger number of rain gauges with longer record durations compared to previous studies (refer to Table 3), which enabled a more accurate evaluation of SPDS performance.

2. Materials and Methods

2.1. The Study Area

The study area covers the whole extent of the Kingdom of Saudi Arabia (KSA). KSA lies between latitudes 16° and 33° N and longitudes 34° and 56° E with an area extent of about 2,150,000 km² and spans about 80% of the Arabian Peninsula. KSA has a western 2250 km shoreline along the Red Sea and an eastern one of 550 km along the Arabian Gulf. The two water bodies are the source of water vapor in the country [60]. KSA's main topographic features is classified into coastal plains, northern and Najd plateaus, the Empty Quarter Desert, the Tuwayq mountains, and Asir Mountains. The highest level in the country is 2990 m above sea level at Asir Mountains [44]. The levels steeply raised from the coastal area and gradually varied to the central area toward Najd Plateau and Arabian Gulf. Figure 1 shows the location and the topography of KSA and the average annual precipitation.

The KSA area is categorized into arid and semi-arid regions [61,62]. The study area has light winds and high temperatures in most areas. Rainfall depths have high spatial and temporal variance, and each season has its distinctive weather patterns. Most rains fall in the winter from October to April [63,64]. The southwestern region is characterized by high rainfall spatial variation due to topographic complexity that triggers convective rain conditions [61,65,66]. Winter rainfall is caused by western winds and the Mediterranean Sea and the Sudan Trough effect [62]. Generally, desert areas have an annual rainfall depth of less than 100 mm, while mountainous areas have rainfall depths ranging from 250 mm to 300 mm [61,62,64].

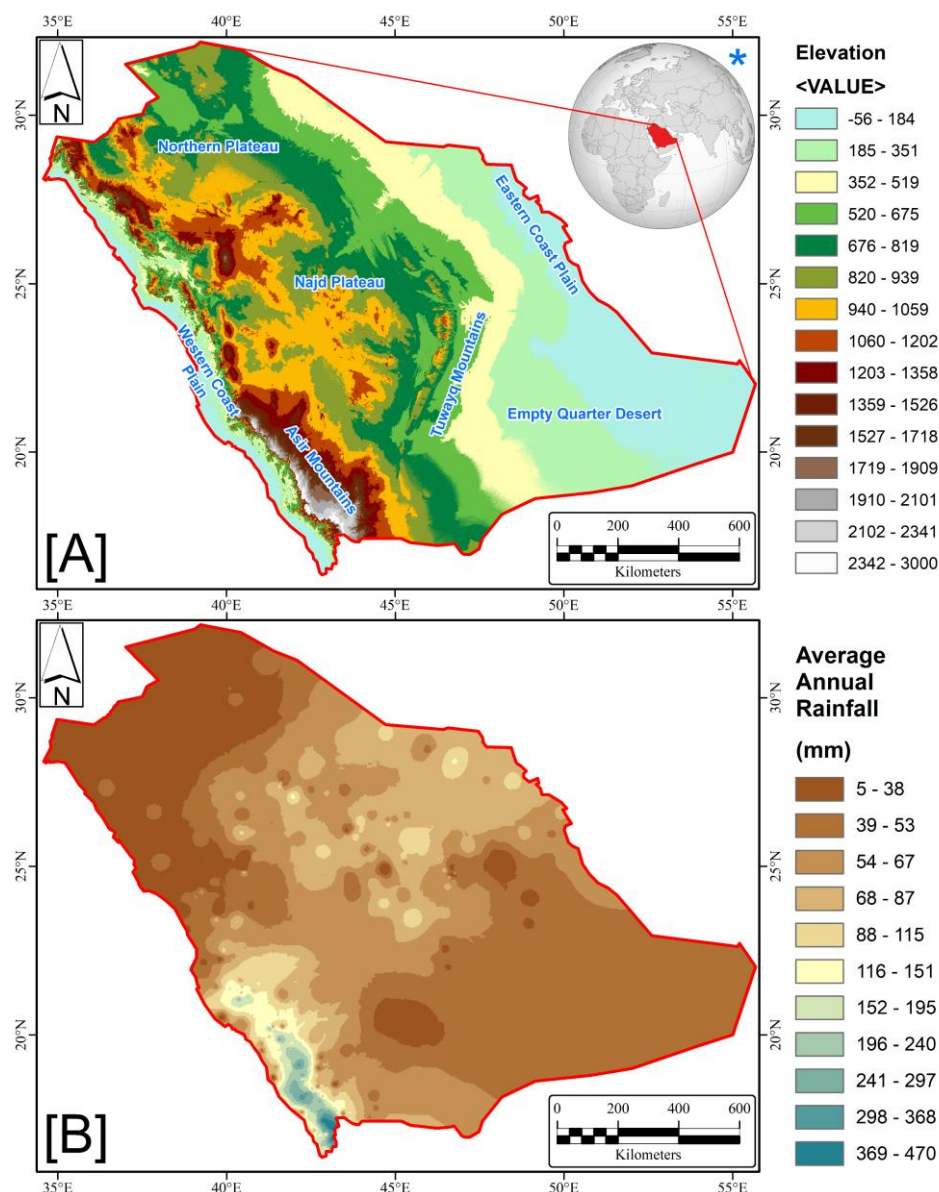


Figure 1. (A) Location and topography of the Kingdom of Saudi Arabia, (B) average annual precipitation (* [https://en.wikipedia.org/wiki/Saudi_Arabia#/media/File:Saudi_Arabia_\(orthographic_projection\).svg](https://en.wikipedia.org/wiki/Saudi_Arabia#/media/File:Saudi_Arabia_(orthographic_projection).svg)), accessed on 5 January 2022.

2.2. Satellite Data

PERSIANN-CDR, CMORPH, CHIRPS V2.0, TMPA 3B42 V7, and GPM IMERG V6 Final Precipitation were selected for the current study. The selected five SPDSs satisfied a minimum of one-day temporal resolution to match the terrestrial rain gauges' records, in addition to the spatial coverage for the study area. The time coverage for each dataset is shown in Figure 2. The following paragraphs briefly describe the characteristic of each precipitation dataset that was used.

Precipitation estimation from remotely sensed information using artificial neural networks (PERSIANN) [17] provides satellite-based precipitation products from 1983 to the near present. Three PERSIANN products are available based on data processing algorithms and spatial and temporal resolutions, namely PERSIANN, PERSIANN-CDR, and PERSIANN-CCS [67]. The PERSIANN products are developed by the Center for Hydro-meteorology and Remote Sensing at the University of California, Irvine, using gridded satellite (GridSat-B1) IR data [68]. The daily/0.25° PERSIANN-CDR dataset from 1983-01-

01 to 2022-09-09 was downloaded for the current study from: (<https://www.ncei.noaa.gov/data/precipitation-persianm/access/>), accessed on 15 October 2022.

NOAA—climate data record (CDR) of climate prediction center (CPC) morphing technique (CMORPH) [15] provides high-resolution quasi-global satellite precipitation estimates. The morphing technique utilizes low orbiter satellite passive microwave (PMW) data to develop the precipitation estimates [69]. The precipitation data covered (60° N–60° S) a region with (0.25°) spatial resolution for daily datasets and 8 km resolution for 30 min temporal resolution datasets. The CMORPH data period extended from 1998 to 2021 [70]. The daily/0.25° CMORPH dataset from 1 January 1998 to 31 December 2021 was downloaded for the current study from: (<https://www.ncei.noaa.gov/data/cmorph-high-resolution-global-precipitation-estimates/access/daily/>), accessed on 8 May 2022.

Climate hazards group infrared precipitation combined with terrestrial stations observations (CHIRPS) is a quasi-global precipitation dataset that covers (50° N–50° S) a region with (0.05°) spatial resolution satellite imagery [19]. CHIRPS relies on long periods of infrared cold cloud duration (CCD) rainfall estimates and ‘smart interpolation’ techniques [69,71]. CHIRPS uses TMPA 3B42 V7 algorithm [72] to calibrate the global CCD rainfall estimates and also builds on interpolated gauge products [73–75]. CHIRPS precipitation data are available in monthly, decadal, pentadal, and daily temporal resolutions by the University of California at Santa Barbara (UCSB), from 1981 to the near present [76]. The daily/0.05° CHIRPS V2.0 dataset from 1 January 1981 to 9 September 2022 was downloaded for the current study from: (https://data.chc.ucsb.edu/products/CHIRPS-2.0/global_daily/netcdf/), accessed on 5 June 2022.

The tropical rainfall measuring mission (TRMM) is the first satellite mission dedicated to tropical and subtropical rainfall studying. TRMM is a joint mission between NASA and the Japan Aerospace Exploration Agency (JAXA). The mission covered more than two-thirds of the world’s area, which falls between $\pm 50^\circ$ of the equator. The satellite flew at a low orbital altitude of about 400 km to detect rainfall. The mission used 5 sensors utilized in the TRMM multi-satellite precipitation analysis algorithm (TMPA) [72]. The TMPA products are found in two temporal scales, TMPA 3B43 monthly precipitation averages and TMPA 3B42 daily and sub-daily (3 h) averages; 3B42 and 3B43 are available in 0.25° spatial resolution [77]. Version 6 and version 7 are available for both TMPA datasets. A considerable number of researchers concluded that TMPA 3B42 V7 significantly improved over TMPA 3B42 V6 [78–82]. The daily/0.25° TMPA 3B42 V7 from 1 January 1998 to 1 January 2020 was downloaded for the current study from: (https://disc.gsfc.nasa.gov/datasets/TRMM_3B42_Daily_7/summary), accessed on 7 April 2022.

The global precipitation measurement mission (GPM) launched on February 2014, was initiated by NASA and JAXA as a successor to the TRMM. GPM provides global precipitation and snow observations through a constellation of international satellite networks [20]. The key advantage of the GPM over the TRMM is the capability of capturing light rain with an intensity of less than 0.5 mm/hour [83]. The GPM estimates were based on the use of an advanced dual frequency precipitation radar (DPR) and multi-channel GPM microwave imager (GMI) attached to a Core Observatory satellite. The COS acted as a reference for the standardization of the different operational satellite measurements [84]. The IMERG version 6 is the latest GPM algorithm that reprocessed the early collected precipitation estimates during the TRMM operation in addition to the current data. GPM covered the globe (90° N–90°S) region with (0.1°) spatial resolution and provided 30 min, 3 h, daily, 3 days, 7 days, and one-month temporal resolutions datasets [85]. The daily/0.1° GPM IMERG V6 final precipitation from 2000-06-01 to 2021-10-01 was downloaded for the current study from: (https://disc.gsfc.nasa.gov/datasets/GPM_3IMERGDF_06/summary), accessed on 7 June 2022.

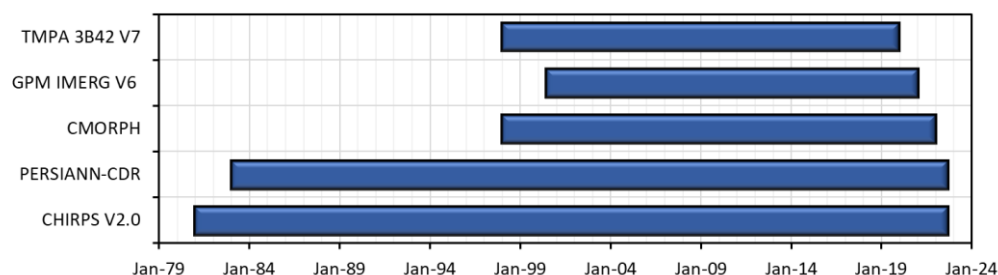


Figure 2. The time coverage for each satellite-based precipitation dataset (SPDS).

2.3. Rain Gauges

Ground rain-gauge data were acquired from the Ministry of Environment of KSA (ME), the Ministry of Water and Agriculture of KSA (MEWA), and the Presidency of Meteorology and Environment of KSA (PME). Among 385 accessed rain gauges, only 324 gauges overlapped with (at least) one year of daily records for each precipitation dataset. The temporal coverage of the data analysis controls the selection of rain gauges based on the available overlap period with the satellite data. In the current study, a minimum of 365 days, 36 months, and 10 years are chosen as an overlapped records period threshold for the daily, monthly, and yearly data analysis, respectively. Additionally, the collector rain gauges were removed during conducting the daily and monthly analyses but considered in the yearly one. The spatial distribution of the selected rain gauges with altitude over KSA zones is shown in Figure 3. The number of rain gauges in each zone and for each analysis time frame is given in Table 4. The variation in the selected rain gauges' density for each analysis period is minor and did not generate a noticeable impact on the density of the rain gauges used over the study area as shown in Figure S1 in the supplementary materials section.

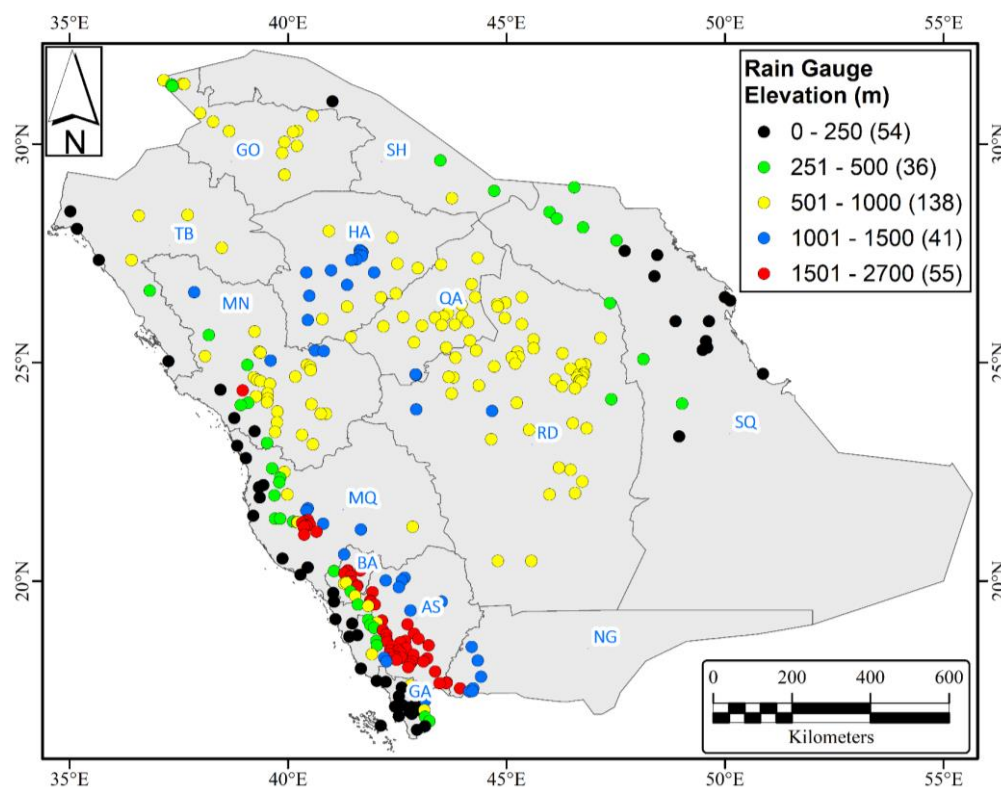


Figure 3. Rain gauges elevations and distribution over KSA administrative zones for different analysis periods.

Table 4. Distribution of rain gauges in the KSA administrative zones.

Zone Name	Zone Code	Total Rain Gauges	Rain Gauges Daily Analysis	Rain Gauges Monthly Analysis	Rain Gauges Yearly Analysis
Holy Makkah	MQ	45	45	45	39
Asir	AS	51	50	50	48
Tabouk	TB	9	9	9	9
Jazan	GA	24	24	24	21
Al-Baha	BA	15	15	15	12
Al-Jouf	GO	17	17	16	14
Madinah	MN	37	25	24	27
Qaseem	QA	23	22	22	19
Al-Sharqiyah	SQ	19	17	16	13
Hail	HA	21	21	21	15
North Region	SH	4	4	4	4
Riyadh	RD	52	52	48	37
Najran	NG	7	3	3	1

2.4. Evaluation of SPDSs

2.4.1. Rain-Gauge Data Screening

In arid and semi-arid regions, near-zero (and zero) values were common as the lower limit of the measurements. Meanwhile, the maximum annual rainfall depths reached high values that may look like an outlier. These high values (outliers) can be attributed to human errors in recording and archiving, device calibration, or errors in reading and recording rainfall depths. Thus, checking the outliers was very important before proceeding with the analyses. Equations (1) and (2) are used to eliminate the outlier measurements from rainfall records [86]. The available rain-gauge data were provided in a list format containing only the date of rainy days and the rain depth in mm, while the remaining days (with no data) were considered dry (i.e., 0 mm/day rainfall depth).

$$\text{Max} = \mu_G + K_m \times \sigma_G \quad (1)$$

$$K_m = 1.055 + 0.981 \times \log N \quad (2)$$

where N is the number of rainy days, and μ_G , and σ_G are the mean and standard deviation of rain gauge records.

In the current study, the SPDSs assessment was carried out using six quantitative statistical metrics and three categorical statistical matrices.

2.4.2. Quantitative Statistical Metrics

Six quantitative statistical metrics were utilized to evaluate the quality of the SPDS. Pearson correlation coefficient (CC), Equation (3), is a scale for the strength of the linear relationship between rain-gauge and SPDS-based values. It ranged between -1 for a perfect inverse linear relation to 1 for a perfect linear relationship. The zero value represented no linear relationship. Further, Nash–Sutcliffe efficiency coefficient (NSE), Equation (4), [87] is a normalized coefficient that considered the ratio between the SPDS residual variance and the rain-gauge measurements variance that varies between $-\infty$ and 1 . Negative NSE value indicated that the mean of the rain-gauge readings was better than the SPDSs as a predictor of rainfall. The perfect match was achieved with $\text{NSE} = 1$. Moreover, Kling–Gupta efficiency score (KGE), Equation (5), [88] is considered an improvement of the NSE [89]. KGE is a composite performance measure that depends on the decomposition of the NSE into its principal components (linear correlation, mean bias, and standard deviation bias). KGE varies between $-\infty$ and 1 , a score of -0.41 represents the KGE value corresponding to the mean observed precipitation benchmark. The range $-0.41 < \text{KGE} < 1$ can be considered reasonable and the perfect match was achieved with $\text{KGE} = 1$ [90]. Relative bias

(RB), Equation (6), represents the systematic error between the satellite data and rain-gauge measurements. Mean absolute error (MAE), Equation (7), represents the average error magnitude in mm. The root mean square error (RMSE) is the standard deviation of the residuals, and the centered root mean square error (RMSE_c), Equation (8), isolates the difference in the means in the assessment of patterns in mm.

$$CC = \frac{\sum_{i=1}^n (S_i - \bar{S}) \cdot (G_i - \bar{G})}{\sqrt{\sum_{i=1}^n (S_i - \bar{S})^2} \cdot \sqrt{\sum_{i=1}^n (G_i - \bar{G})^2}} \tag{3}$$

$$NSE = 1 - \frac{\sum_{i=1}^N (G_i - S_i)^2}{\sum_{i=1}^N (G_i - \bar{G}_i)^2} \tag{4}$$

$$KGE = 1 - \sqrt{(CC - 1)^2 + \left(\frac{\sigma_S}{\sigma_G} - 1\right)^2 + \left(\frac{\mu_S}{\mu_G} - 1\right)^2} \tag{5}$$

$$RB = \frac{\sum_{i=1}^N (S_i - G_i)}{\sum_{i=1}^N G_i} \tag{6}$$

$$MAE = \frac{\sum_{i=1}^N |S_i - G_i|}{N} \tag{7}$$

$$RMSE_c = \sqrt{\frac{1}{N} \sum_{i=1}^N [(S_i - \bar{S}) - (G_i - \bar{G})]^2} = \sqrt{\sigma_S^2 + \sigma_G^2 - 2 \cdot \sigma_S \cdot \sigma_G \cdot CC} \tag{8}$$

where μ_S , and σ_S are the mean and standard deviation of satellite precipitation data.

2.4.3. Categorical Metrics

In addition to the quantitative metrics, the precipitation-capturing capability of each SPDS was evaluated using three categorical metrics, namely (a) the probability of detection (POD), (b) the false alarm ratio (FAR), and (c) the critical success index (CSI) [91]. As per the available daily gauge values, the categorical metrics were calculated in daily temporal resolution based on the number of hits, misses, and false alarm counts as shown in Table 5. POD was the ratio of the correct satellite estimated number of precipitation occurrences to the total number of gauged precipitation events, including the null values, as given in Equation (9), with an optimal value of 1. Additionally, FAR was the ratio of the wrongly estimated precipitation estimates to the total number of satellite-estimated rainfall events, as given in Equation (10), with an optimal value of 0. Lastly, the calculation of the CSI included both missed and false alarm events, as given in Equation (11), with an optimal value of 1. In the current study, 0.5 mm/day was selected as a threshold to confirm the occurrence of rainfall on any day. Figure 4 shows the flow chart of calculating categorical and quantitative metrics.

Table 5. Precipitation contingency table between precipitation gauged data and SPDSs.

		Gauge Data	
		Rain (≥ 0.5 mm/Day)	No Rain (< 0.5 mm/Day)
Satellite Data	Rain (≥ 0.5 mm/day)	Hits (H)	False alarm (F)
	No rain (< 0.5 mm/day)	Miss (M)	Correct negative

$$\text{Probability of Detection (POD)} = \frac{H}{H + M} \tag{9}$$

$$\text{False Alarm Ratio (FAR)} = \frac{F}{H + F} \quad (10)$$

$$\text{Critical Success Index (CSI)} = \frac{H}{H + M + F} \quad (11)$$

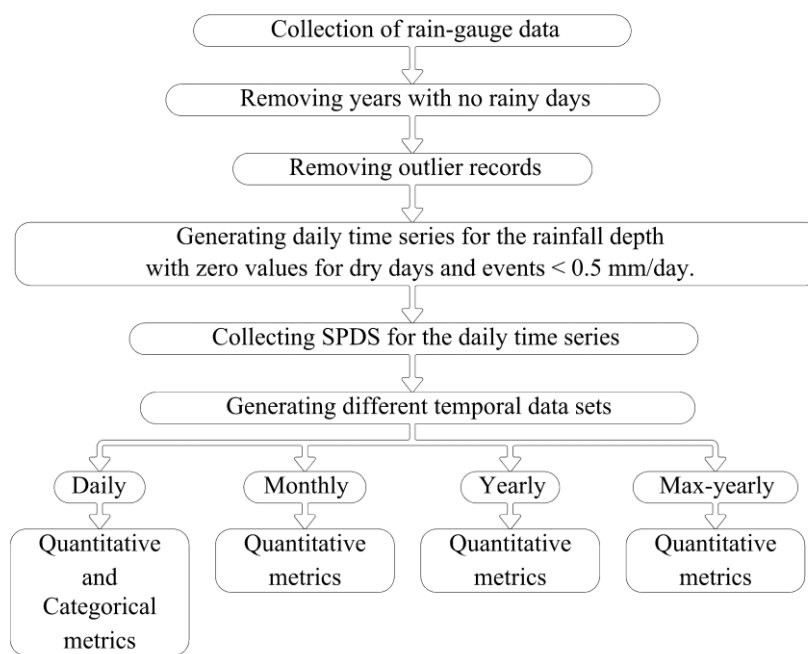


Figure 4. Flow chart for calculating categorical and quantitative metrics.

3. Results and Discussion

The categorical statistical metrics (POD, FAR, and CSI) are calculated for daily precipitation values. The altitude range is classified into six categories (0–250 m), (250–500 m), (500–750 m), (750–1000 m), (1000–1500 m), and (1500–2600 m), in addition to the total range (0–2600 m). The variation of each categorical parameter for each dataset and altitude range is given in Figure 5. GPM IMERG V6 and PERSIANN-CDR SPDSs have the highest POD with an average value of 0.55 for both. CHIRPS V2.0 SPDS has the lowest POD with an average value of 0.31. GPM IMERG V6 has a higher average CSI (0.14) and lower average FAR (0.84) compared to the PERSIANN-CDR SPDS (CSI = 0.1, and FAR = 0.88).

As shown in Figure 5, the major trend for all satellites except minor anomalies is that the best performance (highest POD, CSI, and lowest FAR) is found at 500–1000 m altitude. This trend contradicts previous studies that stated that SPDSs have better performance at low altitudes rather than at high altitudes [92]. Most of the low-altitude rain gauges (0–500 m) are located at the foot of the Red Sea Mountains in the western region and in the vicinity of the Red Sea coast, which is affected by humid weather and seasonal wind. Most stations with an altitude of 500–1000 m are located on Najd and the Northern plateaus in the central and northern regions of KSA. The central area of KSA is relatively flat and has dry weather. Accordingly, it is likely that the effect of the Red Sea seasonal wind, humid weather, and the mountains explain the better performance for 500–750 m rain gauges rather than (0–500 m) rain gauges. Figure 6 shows the variation of GPM IMERG V6 categorical metrics (POD, CSI, and FAR) with altitude. The spatial distribution of the categorical metrics is generated using inverse distance weighted interpolation (IDW) as shown in Figure S2 in the Supplementary Section.

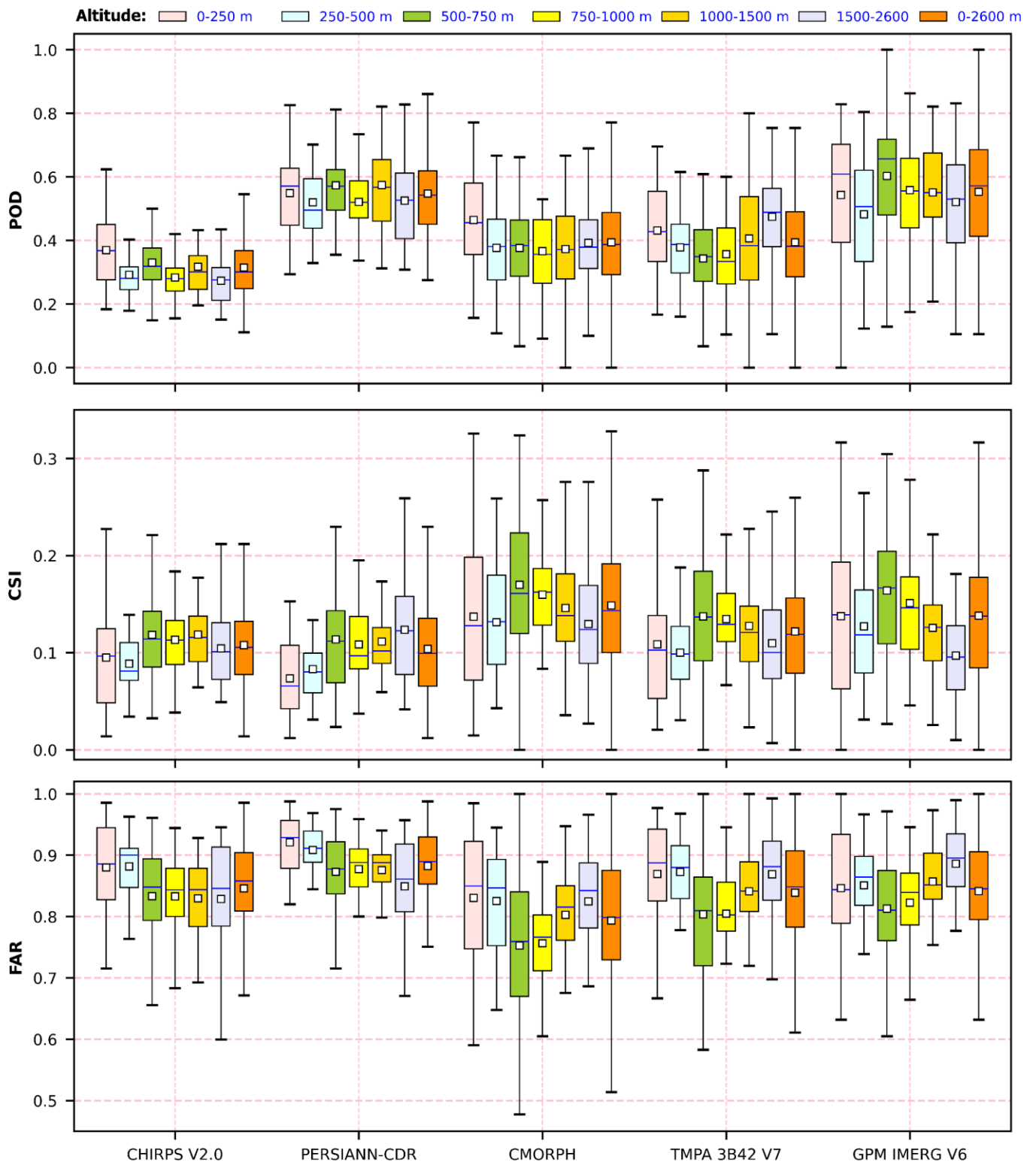


Figure 5. Variation of categorical metrics (POD, CSI, and FAR) with gauge altitude.

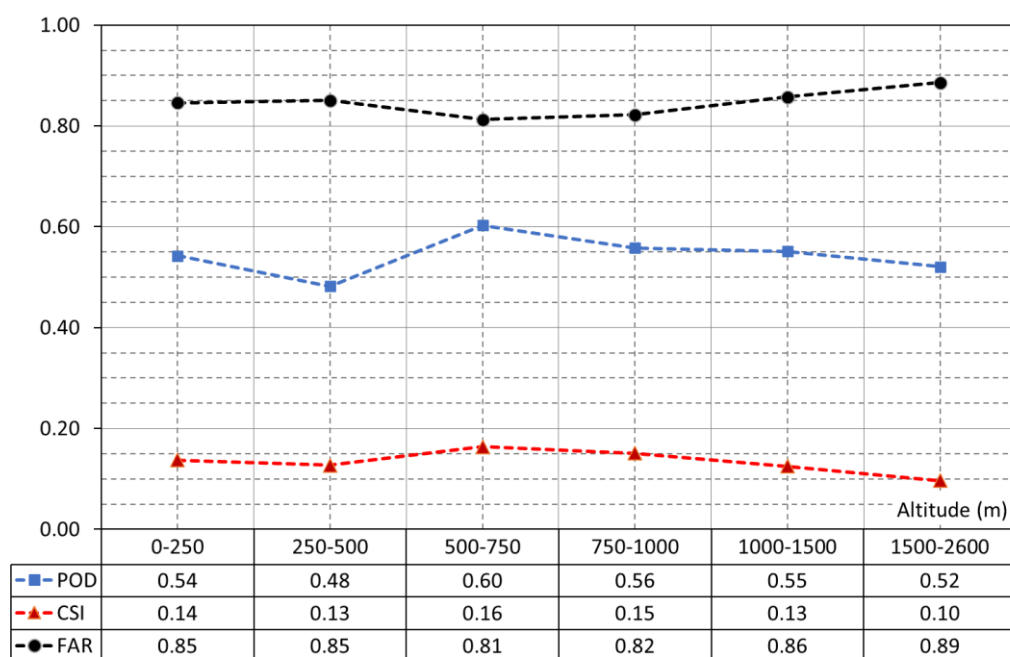


Figure 6. Variation of GPM IMERG V6 categorical metrics (POD, CSI, and FAR) with altitude.

The used six quantitative statistical metrics can be classified into two groups. The first group includes CC, NSE, and KGE, which are utilized to evaluate the SPDSs adequacy to estimate precipitation depth. The second group includes RB, MAE, and RMSEc, which are used to rank the SPDSs adequacy based on error evaluation. All statistical metrics are calculated in daily, monthly, yearly, and maximum yearly temporal resolution for each satellite at each rain gauge location, and the results are then classified based on the altitude of the rain gauge.

The study area is characterized by its large extent, topographic, and climatic variability. Additionally, the distribution of the rain gauges over the study area is not uniform and has a large density variation. To assess the variation of the quantitative statistical metrics over the study area, the IDW technique is utilized to provide $0.05^\circ \times 0.05^\circ$ raster for each parameter over the study area.

The mean value of CC is calculated using ArcGIS zonal statistics spatial analysis. Figure 7 shows the variation of the average CC value over the study area for each satellite and analysis duration. A low correlation for all satellites is found for daily and maximum yearly analyses with the highest value of 0.31 for GPM IMERG V6 in the daily analysis and 0.32 for CMORPH in the maximum yearly analysis. The CHIRPS V2.0 has the lowest correlation coefficient (0.18 and 0.14 for the daily and maximum yearly analysis, respectively). The correlation coefficient slightly improved in the yearly analysis with the highest value of 0.43 for PERSIANN-CDR. The best correlation coefficient for all satellites is found in the monthly analysis with a GPM IMERG V6 average value of 0.58. Figures 8 and 9 show the spatial distribution of CC, NSE, and KGE for daily and monthly rain gauge records. The yearly and maximum yearly record coefficients are shown in Figures S3 and S4 in the Supplementary Section.

The concern of using NSE in this study is that it could not significantly differentiate between variables with low correlations as shown in Figure 8 with an average correlation coefficient of about 0.24 unlike Figure 9 with an average correlation coefficient of about 0.53. Decomposing the NSE to its primary components (linear correlation, mean bias, and standard deviation bias) in the KGE score overcomes this shortcoming. Differentiation between areas with low correlation coefficients could be achieved using KGE as shown in Figure 8.

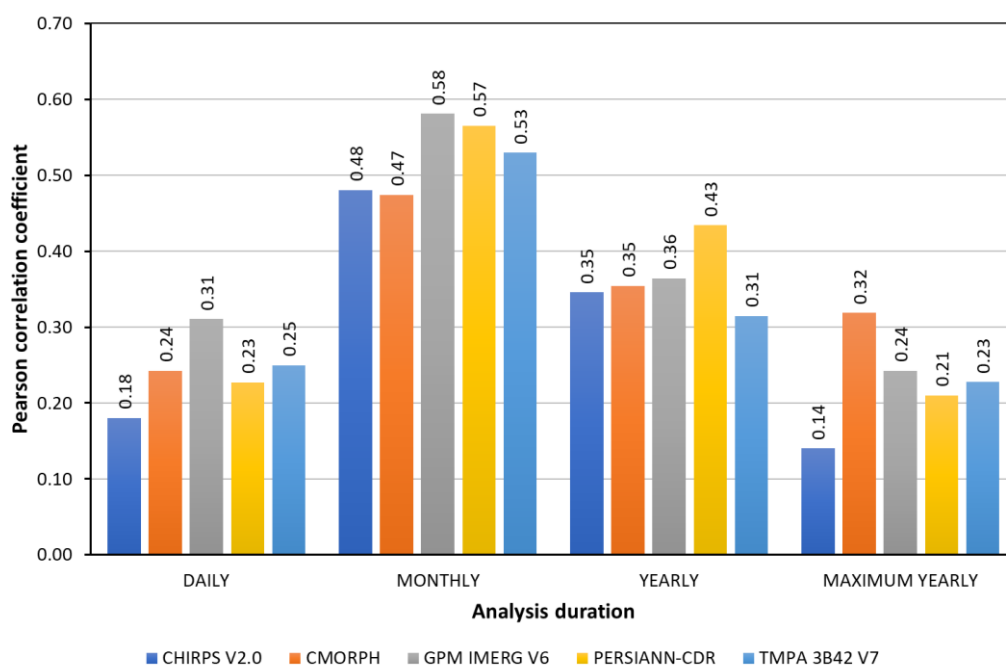


Figure 7. Variation of the Pearson correlation coefficient mean values over the study area.

Figure 10 shows the variation in the monthly CC for all satellites with respect to gauge's altitude. Similar to the categorical metrics, the highest values of the correlation are found at 500–750 m altitude. The variation of the correlation coefficient with gauge altitude for all analysis periods is given in Figure S5 in the Supplementary Section.

The quantitative statistical metrics (i.e., RB, MAE, and RMSEc) provide a different lens for error assessment. The variation of RB, MAE, and RMSEc is given in Figures S6–S9. The root mean square error (RMSE) is the most widely used statistical parameter to quantify the errors. In the current study, Taylor's diagram [93] is utilized to provide a concise summary of the performance of different SPDSs through the graphical plot of the standard deviation and CC for the rain gauges' measurements and SPDSs. The centered root mean square error (RMSEc) is the mean removed RMSE, as given in Equation (8). Figure 11 shows the Taylor diagram for two sample rainfall gauges, namely R119 and A126. These stations were selected to represent the low- and high-intensity area, respectively. In the current study, the RMSEc is proposed as a ranking criterion for the adequacy of the SPDSs, where the satellite with the smallest RMSEc (the nearest one to the rain gauge point in the diagram) will be selected as the best-performing satellite.

The zonal statistics algorithm is applied to calculate the average RMSEc in each zone and the best-performing satellite is highlighted for each analysis duration in Table 6. Based on the minimum obtained, RMSEc, CMORPH, and GPM IMERG V6 have the best performance over most regions in the study area, while TMPA 3B42V7 has the worst performance. Figures S10–S12 in the supplementary section show the variations of the quantitative statistical metrics (RMSEc, MAE, and RB) with respect to the gauge's altitude for each analysis duration. CMORPH has the lowest MAE, RB, and RMSEc for all analysis periods, except the maximum yearly analyses where GPM IMERG V6 has the lowest MAE. The same trend of variation with the gauge's altitude is a similar correlation coefficient and categorical metric where the lowest errors are found at 500–750 m altitude.

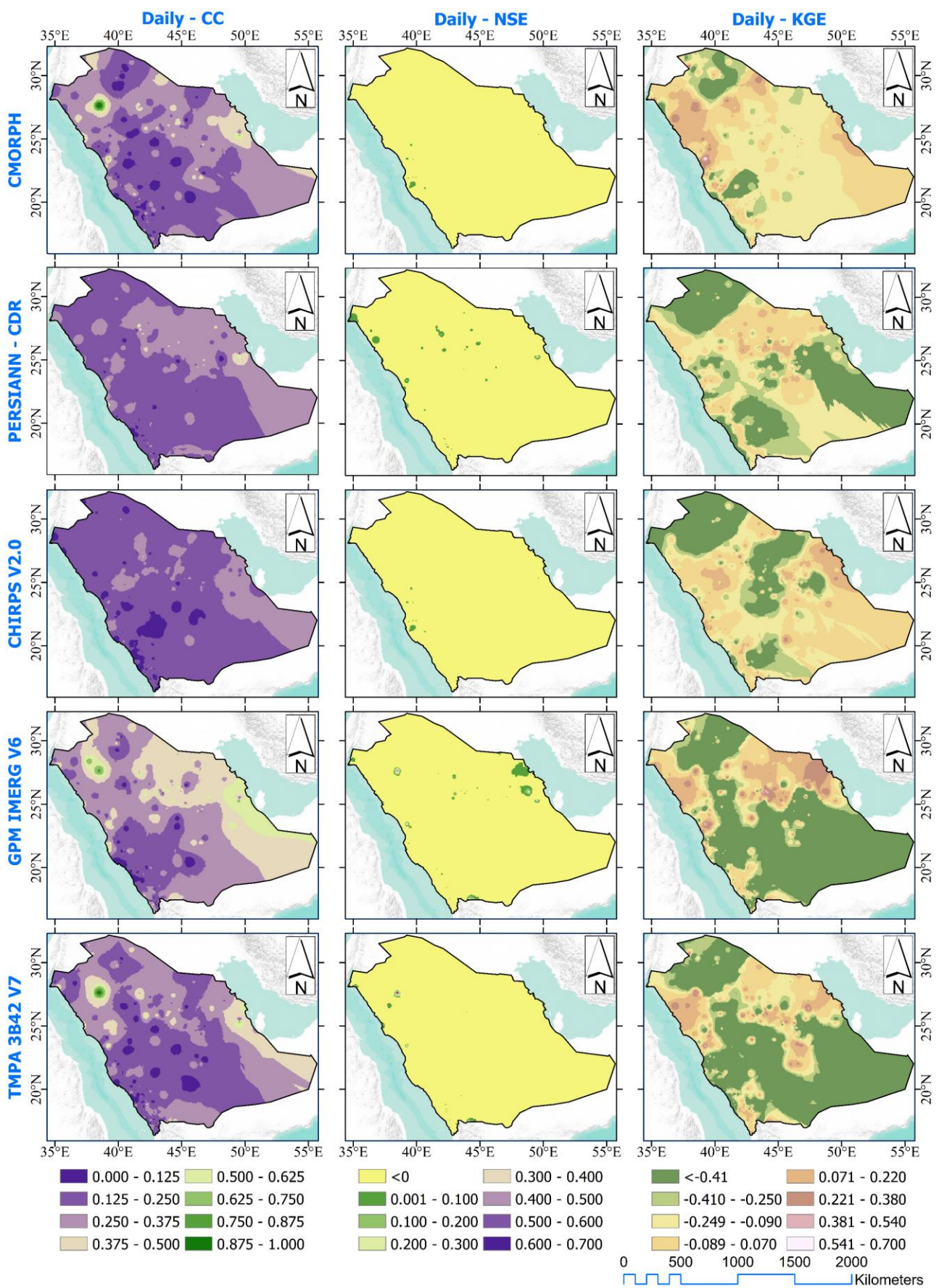


Figure 8. Spatial distribution of daily statistical quantitative metrics (CC, NSE, and KGE) over the study area.

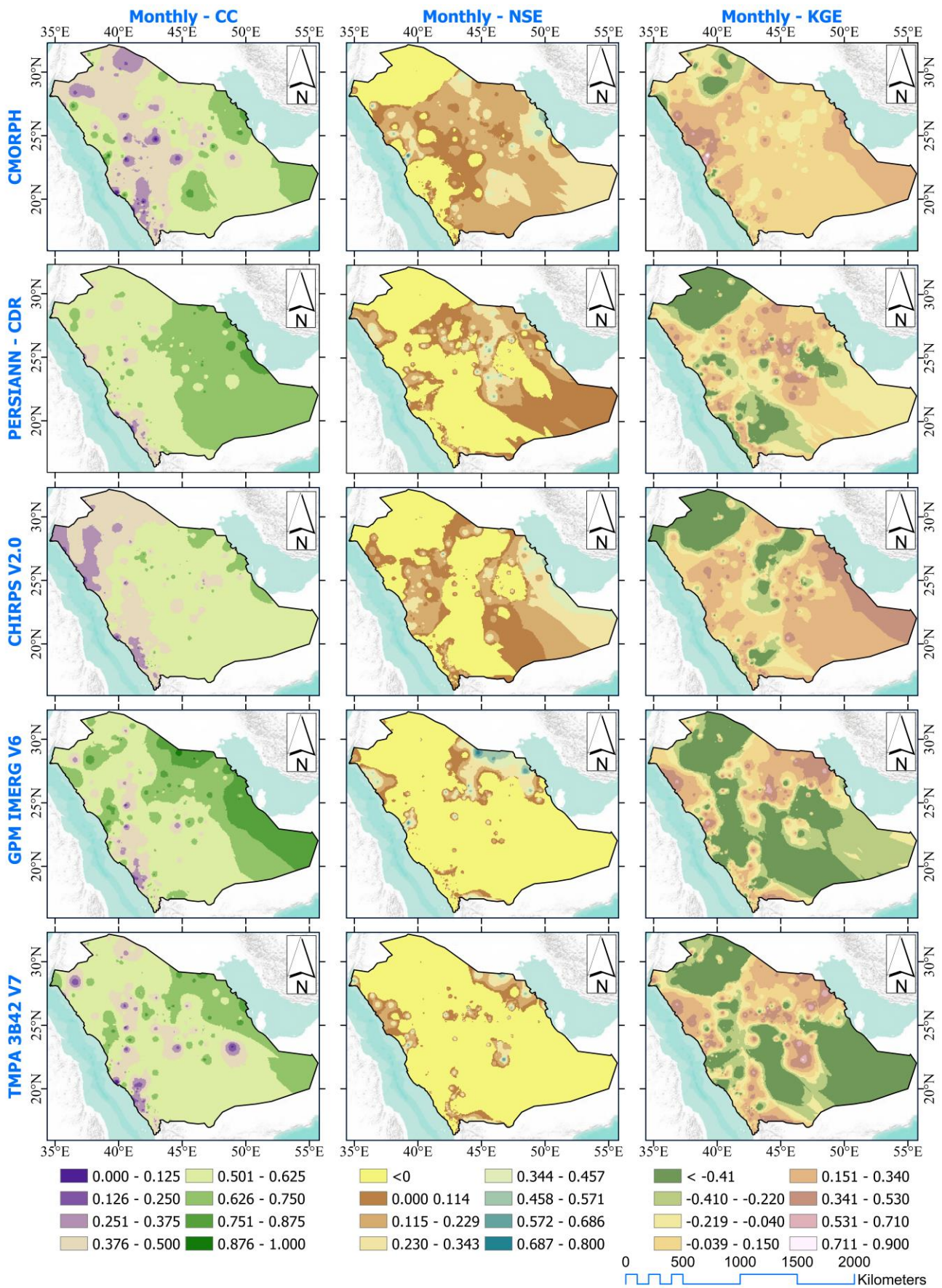


Figure 9. Spatial distribution of monthly statistical quantitative metrics (CC, NSE, and KGE) over the study area.

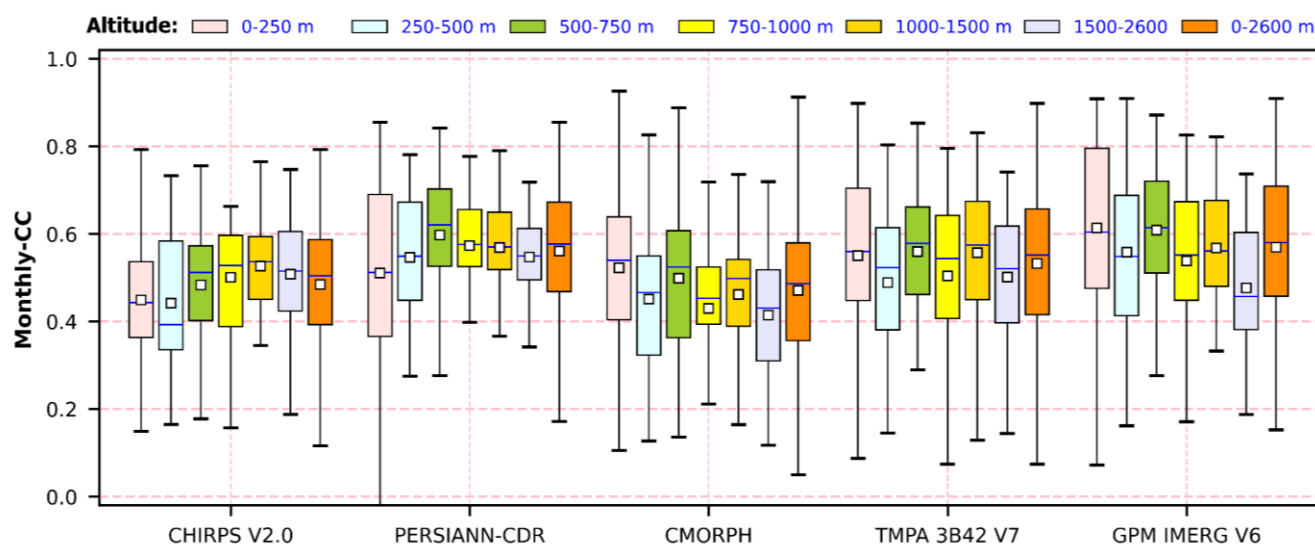


Figure 10. Variation of a monthly correlation coefficient with gauge altitude.

Generally, previous studies did not indicate any overwhelming consensus on the best-performing SPDS, where varying recommendations for the same study area were reported, depending on the number of used rain gauges, temporal coverage, and selected satellite datasets [56,94,95]. In the current study, CMORPH and GPM IMERG V6 had the best performance indices (quantitatively and categorically) across different regions in the KSA. These results agreed to some extent with the previous research conducted on the KSA by (Sultana, and Nasrollahi, 2017) [44] where CMORPH was recommended and by (Mahmoud et al., 2018) [41] where GPM was recommended for the current study area. Further, the altitudinal assessment of SPDS highlighted the better performance at elevations (500–750 m) compared to lower elevations (0–500) found in coastal areas at mountains’ toes, which agrees with (Kim, and Han, 2021) [53] that geographical features affect the quality of CMORPH data. Lastly, the correlation between daily rainfall measurements and SPDS is lower than the correlation at coarser temporal resolutions (e.g., monthly, seasonal, and yearly), as concluded by other previous studies [53,55,57].

Table 6. Variation of RMSEc values for each region in the study area (mm).

Region	Daily	Monthly	Yearly	Max. Yearly	Region	Daily	Monthly	Yearly	Max. Yearly	Satellite
Al-Baha	3.65	23.81	92.57	27.37	Madinah	1.83	11.20	36.77	14.27	CHIRPS
	3.22	22.56	99.86	28.74		1.63	10.50	40.26	14.89	CMORPH
	3.22	21.08	97.68	28.56		1.95	12.04	47.70	15.25	GPM
	3.46	24.48	93.67	27.52		1.75	11.15	39.83	14.46	PERSIANN
	3.45	26.99	111.02	28.23		1.93	11.43	43.99	15.22	TRMM
Al-Jouf	1.46	7.61	25.88	9.08	Najran	2.38	14.54	60.52	13.75	CHIRPS
	1.51	7.93	28.98	12.23		1.94	13.49	58.90	12.43	CMORPH
	1.49	7.32	23.95	11.10		2.09	14.06	74.31	16.00	GPM
	1.27	8.04	25.17	8.45		2.11	13.55	61.37	16.71	PERSIANN
	1.84	9.42	29.11	12.74		2.20	14.43	63.67	20.73	TRMM
Al-Sharqiyah	1.91	10.69	41.94	13.49	North Region	1.80	9.74	34.80	11.50	CHIRPS
	1.37	8.57	33.28	11.88		1.42	8.89	30.65	11.38	CMORPH
	1.76	10.55	38.90	16.37		1.53	7.93	29.16	11.45	GPM
	1.81	10.93	43.41	14.61		1.61	10.11	35.32	11.86	PERSIANN
	2.14	12.92	47.05	18.46		1.84	9.80	34.27	14.22	TRMM
Asir	3.09	20.42	76.54	20.08	Qaseem	2.61	13.77	47.85	18.70	CHIRPS
	2.65	21.25	78.53	18.80		1.64	11.89	36.40	13.94	CMORPH
	2.76	20.18	87.62	17.76		1.97	11.19	39.80	16.53	GPM
	2.81	20.86	81.38	18.67		1.87	12.01	49.48	15.07	PERSIANN
	2.98	21.26	88.48	22.74		2.45	13.11	43.82	16.49	TRMM
Hail	2.15	11.79	38.15	14.12	Riyadh	2.14	12.73	44.46	14.39	CHIRPS

Holy Makkah	1.44	9.33	28.23	11.98	1.45	10.03	36.53	11.82	CMORPH
	1.69	9.73	34.21	14.65	2.00	12.96	49.52	16.91	GPM
	1.81	11.77	41.80	13.46	1.84	12.03	44.67	13.55	PERSIANN
	2.09	11.44	37.85	16.55	2.13	12.28	43.79	16.92	TRMM
	2.63	16.07	56.73	19.67	1.55	8.34	26.53	15.32	CHIRPS
	2.52	16.44	63.75	21.76	1.47	7.60	30.99	16.16	CMORPH
	2.58	16.12	62.51	19.68	1.59	7.56	28.87	12.85	GPM
	2.55	16.87	60.28	20.14	1.43	8.04	27.63	13.64	PERSIANN
	2.78	17.45	64.69	19.60	1.67	8.37	31.82	14.16	TRMM
	Tabouk	4.14	29.79	128.55	20.97	4.32	31.67	126.43	25.26
4.32		31.67	126.43	25.26	4.28	28.37	118.75	21.51	CMORPH
4.28		28.37	118.75	21.51	4.10	32.68	134.32	19.98	GPM
4.10		32.68	134.32	19.98	4.38	29.70	127.99	23.89	PERSIANN
4.38		29.70	127.99	23.89					TRMM

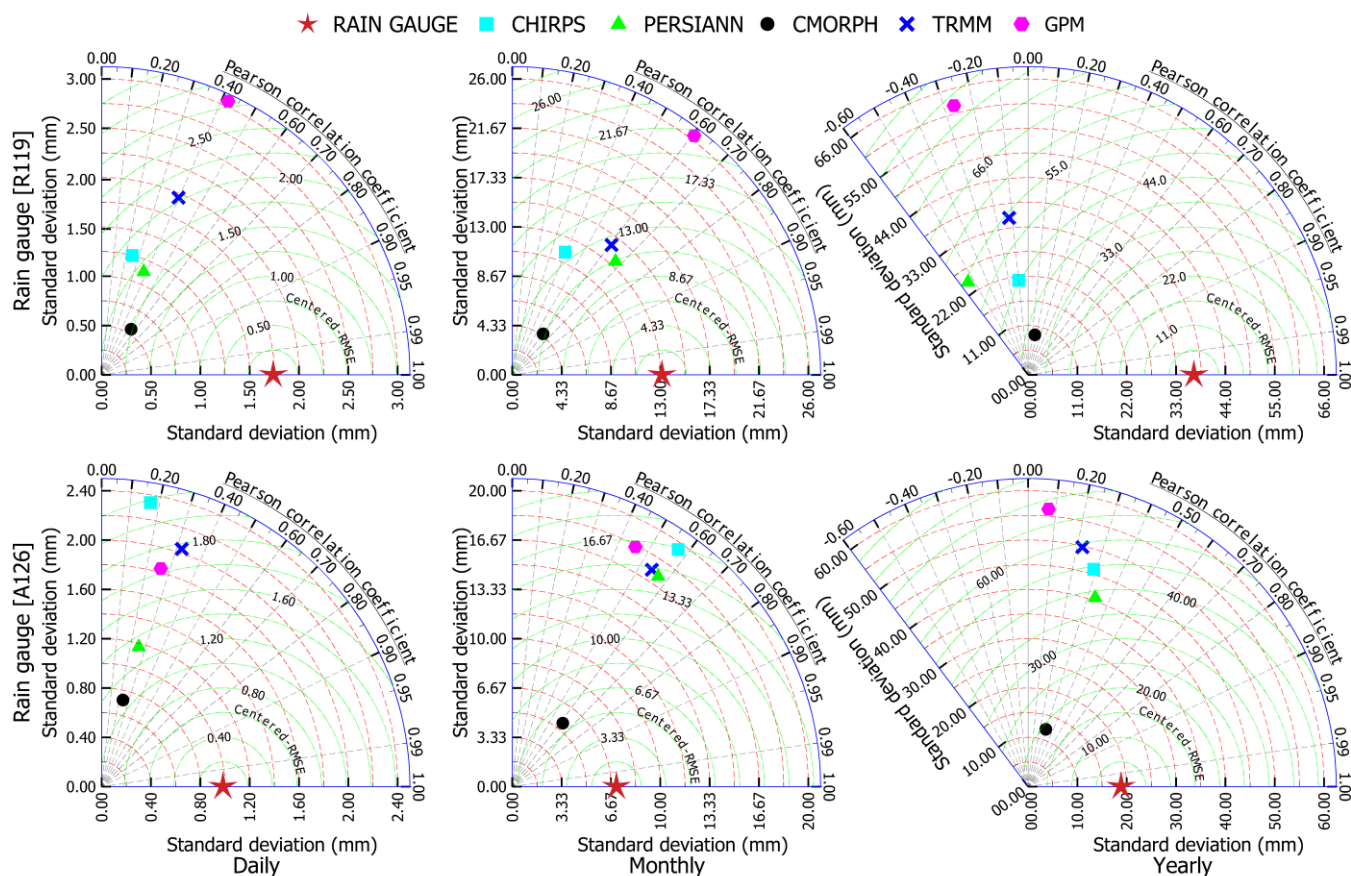
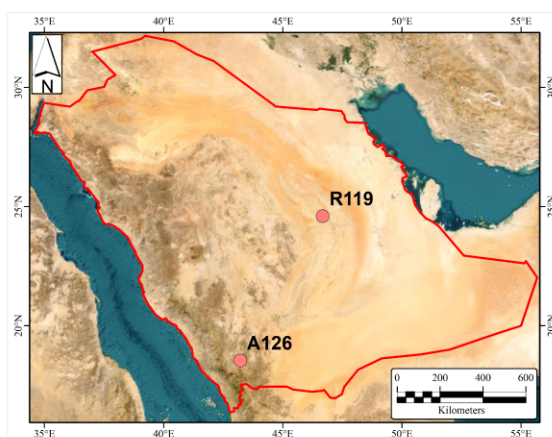


Figure 11. Taylor diagram for rain gauges A126 and R119.

4. Summary and Conclusions

In the current study, the performance of CMORPH, PERSIANN-CDR, CHIRPS V2.0, TMPA 3B42 V7, and GPM IMERG V6 satellite precipitation datasets (SPDSs) were evaluated over the area of the Kingdom of Saudi Arabia (KSA) as an arid region. KSA extends for 2,150,000 km² and occupies most of the Arabian Peninsula as an arid region. The SPDSs were evaluated versus conventional rain-gauge records. The evaluation was conducted for daily, monthly, and yearly temporal resolutions and maximum yearly records. A total of 324 rain gauges' daily data was collected and filtered to remove outliers. A total of 304, 297, and 259 rain gauges out of the 324 was selected for daily, monthly, and yearly analysis temporal resolutions, respectively. The selection of the rain gauges based on satisfying minimum overlapped 365 days, 36 months, and 10 years for daily, monthly, and yearly analysis, respectively.

Several categorical and quantitative metrics were utilized to assess the performance of each SPDS. The categorical metrics included the probability of detection (POD), the false alarm ratio (FAR), and the critical success index (CSI). The quantitative statistical metrics included the Pearson correlation coefficient (CC), Nash–Sutcliffe efficiency coefficient (NSE), Kling–Gupta efficiency score (KGE), relative bias (RB), mean absolute error (MAE), and centered root mean square error (RMSEc). The nine metrics were calculated for each rain gauge, and the results were interpolated over the study area using inverse distance weighted interpolation (IDW). The ArcGIS zonal statistics spatial analysis was used to calculate the average value of each statistical metric for each region of the 13 study area regions. The variation of each statistical metric was assessed at 0–250, 250–500, 500–750, 750–1000, 1000–1500, and 1500–2600 m altitude intervals.

The best performance for all metrics values was found at 500–750 m altitude for all satellites, except minor anomalies. Most of the low-altitude rain gauges (0–500 m) were located at the foot of the Red Sea Mountains in the western region and the vicinity of the Red Sea coast. The majority of stations with (500–750 m) altitude were located on Najd and the Northern plateaus in the central and northern regions of KSA. The effect of the Red Sea seasonal wind and the effect of the mountains may lead to the presence of warm clouds or the evaporation of precipitation before reaching the surface, which can justify the lower performance indicator for 0–500 m altitude. The lowest correlation between the SPDSs and rain gauge records was found in the daily analysis with a maximum value of 0.31 and slightly improved in the maximum yearly and yearly analysis. GPM IMERG V6 had the highest average value of the correlation coefficient of 0.58 in the monthly analysis. Differentiating regions with low correlation coefficients could be achieved using KGE, which was not the case using NSE. Based on error assessment, CMORPH had the lowest MAE, RB, and RMSEc for all analysis periods except for maximum yearly analyses where GPM IMERG V6 had the lowest MAE.

Finally, it can be concluded that the use of daily SPDSs in arid regions could lead to misleading results. The best-performing dataset among the selected SPDSs is the CMORPH with a monthly temporal resolution over the central and northern areas of KSA.

Supplementary Materials: The following supporting information can be downloaded at: <https://www.mdpi.com/article/10.3390/w15010092/s1>, Figure S1. The distribution of the selected rain gauges for each analysis period, Figure S2. Spatial distribution of categorical metrics (POD, CSI, and FAR) over the study area, Figure S3. Spatial distribution of yearly statistical quantitative metrics (CC, NSE, and KGE) over the study area, Figure S4. Spatial distribution of max. yearly statistical quantitative metrics (CC, NSE, and KGE) over the study area, Figure S5. Variation of correlation coefficient with gauge altitude for each analysis duration, Figure S6. Spatial variation of daily RB, MAE, and RMSEc over the study area, Figure S7. Spatial variation of monthly RB, MAE, and RMSEc over the study area, Figure S8. Spatial variation of yearly RB, MAE, and RMSEc over the study area, Figure S9. Spatial variation of maximum yearly RB, MAE, and RMSEc over the study area, Figure S10. Variation of RMSEc with gauge altitude for each analysis duration, Figure S11. Variation of MAE with gauge altitude for each analysis duration, Figure S12. Variation of RB with gauge altitude for each analysis duration.

Author Contributions: Conceptualization, methodology, and analysis A.M.H. and M.S.A.; Software, validation, investigation, resources, and data curation, A.M.H.; writing—original draft preparation, A.M.H. and M.S.A.; writing—review and editing, M.S.A.; visualization, A.M.H. All authors have read and agreed to the published version of the manuscript.

Funding: This research received no external funding.

Data Availability Statement: The datasets used in the current study are free to download from the mentioned links in the manuscript.

Conflicts of Interest: The authors declare no conflict of interest.

References

1. Yuan, F.; Zhang, L.; Wah Win, K.W.; Ren, L.; Zhao, C.; Zhu, Y.; Jiang, S.; Liu, Y. Assessment of GPM and TRMM multi-satellite precipitation products in streamflow simulations in a data sparse mountainous watershed in Myanmar. *Remote Sens.* **2017**, *9*, 302. <https://doi.org/10.3390/rs9030302>.
2. Hou, A.Y.; Kakar, R.K.; Neeck, S.; Azarbarzin, A.A.; Kummerow, C.D.; Kojima, M.; Oki, R.; Nakamura, K.; Iguchi, T. The global precipitation measurement mission. *Bull. Am. Meteorol. Soc.* **2014**, *95*, 701–722. <https://doi.org/10.1175/BAMS-D-13-00164.1>.
3. Petersen, W.A.; Christian, H.J.; Rutledge, S.A. TRMM observations of the global relationship between ice water content and lightning. *Geophys. Res. Lett.* **2005**, *32*, 1–4. <https://doi.org/10.1029/2005GL023236>.
4. Dewan, A.; Hu, K.; Kamruzzaman, M.; Uddin, M.R. Evaluating the spatiotemporal pattern of concentration, aggressiveness and seasonality of precipitation over Bangladesh with time-series Tropical Rainfall Measuring Mission data. In *Extreme Hydroclimatic Events and Multivariate Hazards in a Changing Environment*; Elsevier: Amsterdam, The Netherlands, 2019; pp. 191–219, ISBN 9780128148990.
5. Nashwan, M.S.; Shahid, S.; Dewan, A.; Ismail, T.; Alias, N. Performance of five high resolution satellite-based precipitation products in arid region of Egypt: An evaluation. *Atmos. Res.* **2019**, *236*, 104809. <https://doi.org/10.1016/j.atmosres.2019.104809>.
6. Salman, S.A.; Shahid, S.; Ismail, T.; Ahmed, K.; Wang, X.J. Selection of climate models for projection of spatiotemporal changes in temperature of Iraq with uncertainties. *Atmos. Res.* **2018**, *213*, 509–522. <https://doi.org/10.1016/j.atmosres.2018.07.008>.
7. Nashwan, M.S.; Shahid, S.; Wang, X. Uncertainty in estimated trends using gridded rainfall data: A case study of Bangladesh. *Water* **2019**, *11*, 349. <https://doi.org/10.3390/w11020349>.
8. Abdul Razzaq, Z.T. The feasibility of using TRMM satellite data for missing terrestrial stations in Iraq for mapping the rainfall contour lines. *Civ. Eng. Beyond Limits* **2020**, *3*, 15–19.
9. Himanshu, S.K.; Pandey, A.; Patil, A. Hydrologic Evaluation of the TMPA-3B42V7 Precipitation Data Set over an Agricultural Watershed Using the SWAT Model. *J. Hydrol. Eng.* **2018**, *23*, 05018003. [https://doi.org/10.1061/\(asce\)he.1943-5584.0001629](https://doi.org/10.1061/(asce)he.1943-5584.0001629).
10. Novella, N.S.; Thiaw, W.M. African Rainfall Climatology Version 2 for Famine Early Warning Systems. *J. Appl. Meteorol. Climatol.* **2013**, *52*, 588–606. <https://doi.org/10.1175/JAMC-D-11-0238.1>.
11. Maidment, R.I.; Grimes, D.; Black, E.; Tarnavsky, E.; Young, M.; Greatrex, H.; Allan, R.P.; Stein, T.; Nkonde, E.; Senkunda, S.; et al. A new, long-term daily satellite-based rainfall dataset for operational monitoring in Africa. *Sci. Data* **2017**, *4*, 170063. <https://doi.org/10.1038/sdata.2017.63>.
12. Huffman, G.J.; Behrangi, A.; Bolvin, D.T.; Nelkin, E.J. *GPCP Version 3.2 Daily Precipitation Data Set*; Huffman, G.J., Behrangi, A., Bolvin, D.T., Nelkin, E.J., Eds.; EarthData: Greenbelt, MD, USA, 2022.
13. Xie, P.; Chen, M.; Shi, W. CPC unified gauge-based analysis of global daily precipitation. In *Proceedings of the Preprints, 24th Conference on Hydrology, Atlanta, GA, USA, 17–21 January 2010*; American Meteorological Society: New York, NY, USA; Volume 2.
14. Huffman, G.J.; Bolvin, D.T.; Nelkin, E.J. *TRMM (TMPA) Precipitation L3 1 Day 0.25 Degree × 0.25 Degree V7*; Savtchenko, A., Ed.; EarthData: Greenbelt, MD, USA, 2010.
15. Pingping, X.; Joyce, R.; Wu, S.; Yoo, S.-H.; Yarosh, Y.; Sun, F.; Lin, R. *NOAA Climate Data Record (CDR) of CPC Morphing Technique (CMORPH) High Resolution Global Precipitation Estimates, Version 1*; National Centers for Environmental Information: Asheville, NC, USA, 2019.
16. Hsu, K.L.; Gao, X.; Sorooshian, S.; Gupta, H.V. Precipitation estimation from remotely sensed information using artificial neural networks. *J. Appl. Meteorol.* **1997**, *36*, 1176–1190. [https://doi.org/10.1175/1520-0450\(1997\)036<1176:PEFRSI>2.0.CO;2](https://doi.org/10.1175/1520-0450(1997)036<1176:PEFRSI>2.0.CO;2).
17. Sorooshian, S.; Hsu, K.; Braithwaite, D.; Ashouri, H. *NOAA Climate Data Record (CDR) of Precipitation Estimation from Remotely Sensed Information using Artificial Neural Networks (PERSIANN-CDR), Version 1 Revision 1*; National Centers for Environmental Information: Asheville, NC, USA, 2017.
18. Hong, Y.; Gochis, D.; Cheng, J.T.; Hsu, K.L.; Sorooshian, S. Evaluation of PERSIANN-CCS rainfall measurement using the NAME event rain gauge network. *J. Hydrometeorol.* **2007**, *8*, 469–482. <https://doi.org/10.1175/JHM574.1>.
19. Funk, C.; Peterson, P.; Landsfeld, M.; Pedreros, D.; Verdin, J.; Shukla, S.; Husak, G.; Rowland, J.; Harrison, L.; Hoell, A.; et al. The climate hazards infrared precipitation with stations—A new environmental record for monitoring extremes. *Sci. Data* **2015**, *2*, 150066. <https://doi.org/10.1038/sdata.2015.66>.
20. Wang, K.; Kong, L.; Yang, Z.; Singh, P.; Guo, F.; Xu, Y.; Tang, X.; Hao, J. GPM Annual and Daily Precipitation Data for Real-Time Short-Term Nowcasting: A Pilot Study for a Way Forward in Data Assimilation. *Water* **2021**, *13*, 1422. <https://doi.org/10.3390/w13101422>.

21. Dembélé, M.; Schaeffli, B.; van de Giesen, N.; Mariéthoz, G. Suitability of 17 gridded rainfall and temperature datasets for large-scale hydrological modelling in West Africa. *Hydrol. Earth Syst. Sci.* **2020**, *24*, 5379–5406. <https://doi.org/10.5194/hess-24-5379-2020>.
22. Kumar, B.; Lakshmi, V. Accessing the capability of TRMM 3B42 V7 to simulate streamflow during extreme rain events: Case study for a Himalayan River Basin. *J. Earth Syst. Sci.* **2018**, *127*, 27. <https://doi.org/10.1007/s12040-018-0928-1>.
23. Collischonn, B.; Collischonn, W.; Tucci, C.E.M. Daily hydrological modeling in the Amazon basin using TRMM rainfall estimates. *J. Hydrol.* **2008**, *360*, 207–216. <https://doi.org/10.1016/j.jhydrol.2008.07.032>.
24. Bitew, M.M.; Gebremichael, M. Evaluation of satellite rainfall products through hydrologic simulation in a fully distributed hydrologic model. *Water Resour. Res.* **2011**, *47*, 1–11. <https://doi.org/10.1029/2010WR009917>.
25. Musie, M.; Sen, S.; Srivastava, P. Comparison and evaluation of gridded precipitation datasets for streamflow simulation in data scarce watersheds of Ethiopia. *J. Hydrol.* **2019**, *579*, 124168. <https://doi.org/10.1016/j.jhydrol.2019.124168>.
26. Wang, Q.; Xia, J.; She, D.; Zhang, X.; Liu, J.; Zhang, Y. Assessment of four latest long-term satellite-based precipitation products in capturing the extreme precipitation and streamflow across a humid region of southern China. *Atmos. Res.* **2021**, *257*, 105554. <https://doi.org/10.1016/j.atmosres.2021.105554>.
27. Talchabhadel, R.; Aryal, A.; Kawaike, K.; Yamanoi, K.; Nakagawa, H.; Bhatta, B.; Karki, S.; Thapa, B.R. Evaluation of precipitation elasticity using precipitation data from ground and satellite-based estimates and watershed modeling in Western Nepal. *J. Hydrol. Reg. Stud.* **2021**, *33*, 100768. <https://doi.org/10.1016/j.ejrh.2020.100768>.
28. Abdelmoneim, H.; Soliman, M.R.; Moghazy, H.M. Evaluation of TRMM 3B42V7 and CHIRPS Satellite Precipitation Products as an Input for Hydrological Model over Eastern Nile Basin. *Earth Syst. Environ.* **2020**, *4*, 685–698. <https://doi.org/10.1007/s41748-020-00185-3>.
29. Zhang, Y.; Wu, C.; Yeh, P.J.F.; Li, J.; Hu, B.X.; Feng, P.; Jun, C. Evaluation and comparison of precipitation estimates and hydrologic utility of CHIRPS, TRMM 3B42 V7 and PERSIANN-CDR products in various climate regimes. *Atmos. Res.* **2022**, *265*, 105881. <https://doi.org/10.1016/j.atmosres.2021.105881>.
30. Derin, Y.; Anagnostou, E.; Berne, A.; Borga, M.; Boudevillain, B.; Buytaert, W.; Chang, C.H.; Delrieu, G.; Hong, Y.; Hsu, Y.C.; et al. Multiregional satellite precipitation products evaluation over complex terrain. *J. Hydrometeorol.* **2016**, *17*, 1817–1836. <https://doi.org/10.1175/JHM-D-15-0197.1>.
31. Liu, C.Y.; Aryastana, P.; Liu, G.R.; Huang, W.R. Assessment of satellite precipitation product estimates over Bali Island. *Atmos. Res.* **2020**, *244*, 105032. <https://doi.org/10.1016/j.atmosres.2020.105032>.
32. Helmi, A.M.; Zohny, O. Flash Flood Risk Assessment in Egypt BT. In *Flash Floods in Egypt*; Negm, A.M., Ed.; Springer International Publishing: Berlin/Heidelberg, Germany, 2020; pp. 253–312, ISBN 978-3-030-29635-3.
33. Youssif, M.M.A. Hydrological Study of Large Wadies in Arid and Semi Arid Areas Case Study: Wadi El-Arish, Northern Sinai, Egypt. Master's Thesis, Cairo University, Cairo, Egypt, 2008.
34. Hamdi, E.Y. Precipitation Analysis and Hydrological Modeling in Arid Regions. Master's Thesis, Cairo University, Cairo, Egypt, 2005.
35. Javanmard, S.; Yatagai, A.; Nodzu, M.I.; Bodaghamali, J.; Kawamoto, H. Comparing high-resolution gridded precipitation data with satellite rainfall estimates of TRMM-3B42 over Iran. *Adv. Geosci.* **2010**, *25*, 119–125. <https://doi.org/10.5194/adgeo-25-119-2010>.
36. Miao, C.; Ashouri, H.; Hsu, K.L.; Sorooshian, S.; Duan, Q. Evaluation of the PERSIANN-CDR daily rainfall estimates in capturing the behavior of extreme precipitation events over China. *J. Hydrometeorol.* **2015**, *16*, 1387–1396. <https://doi.org/10.1175/JHM-D-14-0174.1>.
37. Abdulrida, M.A.; Al-Jumaily, K.J. Comparisons of Monthly Rainfall Data with Satellite Estimates of TRMM 3B42 over Iraq. *Int. J. Sci. Res. Publ.* **2016**, *6*, 494–501.
38. Moazami, S.; Golian, S.; Hong, Y.; Sheng, C.; Kavianpour, M.R. Comprehensive evaluation of four high-resolution satellite precipitation products under diverse climate conditions in Iran. *Hydrol. Sci. J.* **2016**, *61*, 420–440. <https://doi.org/10.1080/02626667.2014.987675>.
39. Prakash, S.; Mitra, A.K.; AghaKouchak, A.; Liu, Z.; Norouzi, H.; Pai, D.S. A preliminary assessment of GPM-based multi-satellite precipitation estimates over a monsoon dominated region. *J. Hydrol.* **2018**, *556*, 865–876. <https://doi.org/10.1016/j.jhydrol.2016.01.029>.
40. Bai, L.; Shi, C.; Li, L.; Yang, Y.; Wu, J. Accuracy of CHIRPS Satellite-Rainfall Products over Mainland China. *Remote Sens.* **2018**, *10*, 362. <https://doi.org/10.3390/rs10030362>.
41. Mahmoud, M.T.; Al-Zahrani, M.A.; Sharif, H.O. Assessment of global precipitation measurement satellite products over Saudi Arabia. *J. Hydrol.* **2018**, *559*, 1–12. <https://doi.org/10.1016/j.jhydrol.2018.02.015>.
42. Wei, G.; Lü, H.; Crow, W.T.; Zhu, Y.; Wang, J.; Su, J. Comprehensive Evaluation of GPM-IMERG, CMORPH, and TMPA Precipitation Products with Gauged Rainfall over Mainland China. *Adv. Meteorol.* **2018**, *2018*, 3024190. <https://doi.org/10.1155/2018/3024190>.
43. Wang, C.; Tang, G.; Han, Z.; Guo, X.; Hong, Y. Global intercomparison and regional evaluation of GPM IMERG Version-03, Version-04 and its latest Version-05 precipitation products: Similarity, difference and improvements. *J. Hydrol.* **2018**, *564*, 342–356. <https://doi.org/10.1016/j.jhydrol.2018.06.064>.
44. Sultana, R.; Nasrollahi, N. Evaluation of remote sensing precipitation estimates over Saudi Arabia. *J. Arid Environ.* **2018**, *151*, 90–103. <https://doi.org/10.1016/j.jaridenv.2017.11.002>.
45. Nashwan, M.S.; Shahid, S.; Wang, X. Assessment of satellite-based precipitation measurement products over the hot desert climate of Egypt. *Remote Sens.* **2019**, *101*, 555. <https://doi.org/10.3390/rs11050555>.
46. Fang, J.; Yang, W.; Luan, Y.; Du, J.; Lin, A.; Zhao, L. Evaluation of the TRMM 3B42 and GPM IMERG products for extreme precipitation analysis over China. *Atmos. Res.* **2019**, *223*, 24–38. <https://doi.org/10.1016/j.atmosres.2019.03.001>.
47. Shukla, A.K.; Ojha, C.S.P.; Singh, R.P.; Pal, L.; Fu, D. Evaluation of TRMM precipitation dataset over Himalayan Catchment: The upper Ganga Basin, India. *Water* **2019**, *11*, 613. <https://doi.org/10.3390/w11030613>.

48. Bruster-Flores, J.L.; Ortiz-Gómez, R.; Ferriño-Fierro, A.L.; Guerra-Cobián, V.H.; Burgos-Flores, D.; Lizárraga-Mendiola, L.G. Evaluation of precipitation estimates CMORPH-CRT on regions of Mexico with different climates. *Water* **2019**, *11*, 1722. <https://doi.org/10.3390/w11081722>.
49. Gumindoga, W.; Rientjes, T.H.M.; Haile, A.T.; Makurira, H.; Reggiani, P. Performance evaluation of CMORPH satellite precipitation product in the Zambezi Basin. *Int. J. Remote Sens.* **2019**, *40*, 7730–7749. <https://doi.org/10.1080/01431161.2019.1602791>.
50. Yang, X.; Lu, Y.; Tan, M.L.; Li, X.; Wang, G.; He, R. Nine-year systematic evaluation of the GPM and TRMM precipitation products in the shuaishui river basin in east-central China. *Remote Sens.* **2020**, *12*, 1042. <https://doi.org/10.3390/rs12061042>.
51. Cavalcante, R.B.L.; da Ferreira, D.B.S.; Pontes, P.R.M.; Tedeschi, R.G.; da Costa, C.P.W.; de Souza, E.B. Evaluation of extreme rainfall indices from CHIRPS precipitation estimates over the Brazilian Amazonia. *Atmos. Res.* **2020**, *238*, 104879. <https://doi.org/10.1016/j.atmosres.2020.104879>.
52. Nwachukwu, P.N.; Satge, F.; El Yacoubi, S.; Pinel, S.; Bonnet, M.P. From trmm to GPM: How reliable are satellite-based precipitation data across Nigeria? *Remote Sens.* **2020**, *12*, 3964. <https://doi.org/10.3390/rs12233964>.
53. Kim, J.; Han, H. Evaluation of the CMORPH high-resolution precipitation product for hydrological applications over South Korea. *Atmos. Res.* **2021**, *258*, 105650. <https://doi.org/10.1016/j.atmosres.2021.105650>.
54. Geleta, C.D.; Deressa, T.A. Evaluation of Climate Hazards Group InfraRed Precipitation Station (CHIRPS) satellite-based rainfall estimates over Finchaa and Neshe Watersheds, Ethiopia. *Eng. Reports* **2021**, *3*, e12338. <https://doi.org/10.1002/eng2.12338>.
55. Yang, W.T.; Fu, S.M.; Sun, J.H.; Zheng, F.; Wei, J.; Ma, Z. Comparative Evaluation of the Performances of TRMM-3B42 and Climate Prediction Centre Morphing Technique (CMORPH) Precipitation Estimates over Thailand. *J. Meteorol. Soc. Jpn.* **2021**, *99*, 1525–1546. <https://doi.org/10.2151/JMSJ.2021-074>.
56. Yu, S.; Lu, F.; Zhou, Y.; Wang, X.; Wang, K.; Song, X.; Zhang, M. Evaluation of Three High-Resolution Remote Sensing Precipitation Products on the Tibetan Plateau. *Water* **2022**, *14*, 2169. <https://doi.org/10.3390/w14142169>.
57. Anjum, M.N.; Irfan, M.; Waseem, M.; Leta, M.K.; Niazi, U.M.; Rahman, S.U.; Ghanim, A.; Mukhtar, M.A.; Nadeem, M.U. Assessment of PERSIANN-CCS, PERSIANN-CDR, SM2RAIN-ASCAT, and CHIRPS-2.0 Rainfall Products over a Semi-Arid Subtropical Climatic Region. *Water* **2022**, *14*, 147. <https://doi.org/10.3390/w14020147>.
58. Pai, D.S.; Rajeevan, M.; Sreejith, O.P.; Mukhopadhyay, B.; Satbha, N.S. Development of a new high spatial resolution (0.25° × 0.25°) long period (1901–2010) daily gridded rainfall data set over India and its comparison with existing data sets over the region. *MAUSAM* **2014**, *65*, 1–18. <https://doi.org/10.54302/mausam.v65i1.851>.
59. Mahmoud, M.T.; Mohammed, S.A.; Hamouda, M.A.; Mohamed, M.M. Impact of topography and rainfall intensity on the accuracy of imerg precipitation estimates in an arid region. *Remote Sens.* **2021**, *13*, 13. <https://doi.org/10.3390/rs13010013>.
60. Al-Ahmadi, K.; Al-Ahmadi, S. Rainfall-altitude relationship in Saudi Arabia. *Adv. Meteorol.* **2013**, *2013*, 363029. <https://doi.org/10.1155/2013/363029>.
61. Al-Zahrani, M.; Husain, T. An algorithm for designing a precipitation network in the south-western region of Saudi Arabia. *J. Hydrol.* **1998**, *205*, 205–216. [https://doi.org/10.1016/S0022-1694\(97\)00153-4](https://doi.org/10.1016/S0022-1694(97)00153-4).
62. Hag-Elsafi, S.; El-Tayib, M. Spatial and statistical analysis of rainfall in the Kingdom of Saudi Arabia from 1979 to 2008. *Weather* **2016**, *71*, 262–266. <https://doi.org/10.1002/wea.2783>.
63. Almazroui, M. Calibration of TRMM rainfall climatology over Saudi Arabia during 1998–2009. *Atmos. Res.* **2011**, *99*, 400–414. <https://doi.org/10.1016/j.atmosres.2010.11.006>.
64. Hasanean, H.; Almazroui, M. Rainfall: Features and variations over Saudi Arabia, a review. *Climate* **2015**, *3*, 578–626. <https://doi.org/10.3390/cli3030578>.
65. Abdullah, M.A.; Almazroui, M. Climatological study of the southwestern region of Saudi Arabia. I. Rainfall analysis. *Clim. Res.* **1998**, *9*, 213–223.
66. Subyani, A.M. Geostatistical study of annual and seasonal mean rainfall patterns in southwest Saudi Arabia/Distribution géostatique de la pluie moyenne annuelle et saisonnière dans le Sud-Ouest de l'Arabie Saoudite. *Hydrol. Sci. J.* **2004**, *49*, 803–816. <https://doi.org/10.1623/hysj.49.5.803.55137>.
67. Nguyen, P.; Ombadi, M.; Sorooshian, S.; Hsu, K.; AghaKouchak, A.; Braithwaite, D.; Ashouri, H.; Thorstensen, A.R. The PERSIANN family of global satellite precipitation data: A review and evaluation of products. *Hydrol. Earth Syst. Sci.* **2018**, *22*, 5801–5816. <https://doi.org/10.5194/hess-22-5801-2018>.
68. Hsu, K.; Ashouri, H.; Braithwaite, D.; Sorooshian, S. *Climate Algorithm Theoretical Basis Document (C-ATBD)—Precipitation—PERSIANN-CDR*; National Oceanic and Atmospheric Administration: Washington, DC, USA, 2014.
69. Joyce, R.J.; Janowiak, J.E.; Arkin, P.A.; Xie, P. CMORPH: A Method that Produces Global Precipitation Estimates from Passive Microwave and Infrared Data at High Spatial and Temporal Resolution. *J. Hydrometeorol.* **2004**, *5*, 487–503. [https://doi.org/10.1175/1525-7541\(2004\)005<0487:CAMTPG>2.0.CO;2](https://doi.org/10.1175/1525-7541(2004)005<0487:CAMTPG>2.0.CO;2).
70. Koutsouris, A.J.; Chen, D.; Lyon, S.W. Comparing global precipitation data sets in eastern Africa: A case study of Kilombero Valley, Tanzania. *Int. J. Climatol.* **2016**, *36*, 2000–2014. <https://doi.org/10.1002/joc.4476>.
71. Willmott, C.J.; Robeson, S.M. Climatologically aided interpolation (CAI) of terrestrial air temperature. *Int. J. Climatol.* **1995**, *15*, 221–229. <https://doi.org/10.1002/joc.3370150207>.
72. Huffman, G.J.; Adler, R.F.; Bolvin, D.T.; Gu, G.; Nelkin, E.J.; Bowman, K.P.; Hong, Y.; Stocker, E.F.; Wolff, D.B. The TRMM Multisatellite Precipitation Analysis (TMPA): Quasi-global, multiyear, combined-sensor precipitation estimates at fine scales. *J. Hydrometeorol.* **2007**, *8*, 38–55. <https://doi.org/10.1175/JHM560.1>.

73. Schneider, U.; Becker, A.; Finger, P.; Meyer-Christoffer, A.; Ziese, M.; Rudolf, B. GPCP's new land surface precipitation climatology based on quality-controlled in situ data and its role in quantifying the global water cycle. *Theor. Appl. Climatol.* **2014**, *115*, 15–40. <https://doi.org/10.1007/s00704-013-0860-x>.
74. Harris, I.; Jones, P.D.; Osborn, T.J.; Lister, D.H. Updated high-resolution grids of monthly climatic observations—The CRU TS3.10 Dataset. *Int. J. Climatol.* **2014**, *34*, 623–642. <https://doi.org/10.1002/joc.3711>.
75. Becker, A.; Finger, P.; Meyer-Christoffer, A.; Rudolf, B.; Schamm, K.; Schneider, U.; Ziese, M. A description of the global land-surface precipitation data products of the Global Precipitation Climatology Centre with sample applications including centennial (trend) analysis from 1901–present. *Earth Syst. Sci. Data* **2013**, *5*, 71–99. <https://doi.org/10.5194/essd-5-71-2013>.
76. Paredes-Trejo, F.; Barbosa, H.A.; Kumar, T.V.L.; Thakur, M.K.; de Oliveira Buriti, C. Assessment of the CHIRPS-Based Satellite Precipitation Estimates. In *Inland Waters*; Devlin, A., Pan, J., Shah, M.M., Eds.; IntechOpen: Rijeka, Croatia, 2020.
77. NASA. Global Precipitation Measurement. Available online: <https://gpm.nasa.gov/missions/TRMM/satellite/PR> (accessed on 7 April 2022).
78. Liu, Z. Comparison of versions 6 and 7 3-hourly TRMM multi-satellite precipitation analysis (TMPA) research products. *Atmos. Res.* **2015**, *163*, 91–101. <https://doi.org/10.1016/j.atmosres.2014.12.015>.
79. Chen, S.; Hong, Y.; Cao, Q.; Gourley, J.J.; Kirstetter, P.E.; Yong, B.; Tian, Y.; Zhang, Z.; Shen, Y.; Hu, J.; et al. Similarity and difference of the two successive V6 and V7 TRMM multisatellite precipitation analysis performance over China. *J. Geophys. Res. Atmos.* **2013**, *118*, 13060–13074. <https://doi.org/10.1002/2013JD019964>.
80. Yong, B.; Chen, B.; Gourley, J.J.; Ren, L.; Hong, Y.; Chen, X.; Wang, W.; Chen, S.; Gong, L. Intercomparison of the Version-6 and Version-7 TMPA precipitation products over high and low latitudes basins with independent gauge networks: Is the newer version better in both real-time and post-real-time analysis for water resources and hydrologic ext. *J. Hydrol.* **2014**, *508*, 77–87. <https://doi.org/10.1016/j.jhydrol.2013.10.050>.
81. Prakash, S.; Mitra, A.K.; Momin, I.M.; Pai, D.S.; Rajagopal, E.N.; Basu, S. Comparison of TMPA-3B42 versions 6 and 7 precipitation products with gauge-based data over India for the southwest monsoon period. *J. Hydrometeorol.* **2015**, *16*, 346–362. <https://doi.org/10.1175/JHM-D-14-0024.1>.
82. Qiao, L.; Hong, Y.; Chen, S.; Zou, C.B.; Gourley, J.J.; Yong, B. Performance assessment of the successive Version 6 and Version 7 TMPA products over the climate-transitional zone in the southern Great Plains, USA. *J. Hydrol.* **2014**, *513*, 446–456. <https://doi.org/10.1016/j.jhydrol.2014.03.040>.
83. Xu, F.; Guo, B.; Ye, B.; Ye, Q.; Chen, H.; Ju, X.; Guo, J.; Wang, Z. Systematical Evaluation of GPM IMERG and TRMM 3B42V7 Precipitation Products in the Huang-Huai-Hai Plain, China. *Remote Sens.* **2019**, *11*, 697. <https://doi.org/10.3390/rs11060697>.
84. Skofronick-Jackson, G.; Petersen, W.A.; Berg, W.; Kidd, C.; Stocker, E.F.; Kirschbaum, D.B.; Kakar, R.; Braun, S.A.; Huffman, G.J.; Iguchi, T.; et al. The global precipitation measurement (GPM) mission for science and Society. *Bull. Am. Meteorol. Soc.* **2017**, *98*, 1679–1695. <https://doi.org/10.1175/BAMS-D-15-00306.1>.
85. Huffman, G.; Bolvin, D.; Braithwaite, D.; Hsu, K.; Joyce, R.; Kidd, C.; Nelkin, E.; Sorooshian, S.; Tan, J.; Xie, P. *NASA GPM Integrated Multi-Satellite Retrievals for GPM (IMERG) Algorithm Theoretical Basis Document (ATBD) Version 06*; National Aeronautics and Space Administration: Washington, DC, USA, 2020.
86. Haan, C.T. *Statistical Methods in Hydrology*, 2nd ed.; Iowa State Press: Ames, IA, USA, 2002; ISBN 0813815037.
87. Nash, J.E.; Sutcliffe, J.V. River flow forecasting through conceptual models part I—A discussion of principles. *J. Hydrol.* **1970**, *10*, 282–290. [https://doi.org/10.1016/0022-1694\(70\)90255-6](https://doi.org/10.1016/0022-1694(70)90255-6).
88. Gupta, H.V.; Kling, H.; Yilmaz, K.K.; Martinez, G.F. Decomposition of the mean squared error and NSE performance criteria: Implications for improving hydrological modelling. *J. Hydrol.* **2009**, *377*, 80–91. <https://doi.org/10.1016/j.jhydrol.2009.08.003>.
89. Pool, S.; Vis, M.; Seibert, J. Evaluating model performance: Towards a non-parametric variant of the Kling-Gupta efficiency. *Hydrol. Sci. J.* **2018**, *63*, 1941–1953. <https://doi.org/10.1080/02626667.2018.1552002>.
90. Knoben, W.J.M.; Freer, J.E.; Woods, R.A. Technical note: Inherent benchmark or not? Comparing Nash–Sutcliffe and Kling–Gupta efficiency scores. *Hydrol. Earth Syst. Sci.* **2019**, *23*, 4323–4331. <https://doi.org/10.5194/hess-23-4323-2019>.
91. Schaefer, J.T. The Critical Success Index as an Indicator of Warning Skill. *Weather Forecast.* **1990**, *5*, 570–575. [https://doi.org/10.1175/1520-0434\(1990\)005<0570:TCSIAA>2.0.CO;2](https://doi.org/10.1175/1520-0434(1990)005<0570:TCSIAA>2.0.CO;2).
92. Zambrano-Bigiarini, M.; Nauditt, A.; Birkel, C.; Verbist, K.; Ribbe, L. Temporal and spatial evaluation of satellite-based rainfall estimates across the complex topographical and climatic gradients of Chile. *Hydrol. Earth Syst. Sci.* **2017**, *21*, 1295–1320. <https://doi.org/10.5194/hess-21-1295-2017>.
93. Taylor, K.E. Summarizing multiple aspects of model performance in a single diagram. *J. Geophys. Res. Atmos.* **2001**, *106*, 7183–7192. <https://doi.org/10.1029/2000JD900719>.
94. Lin, Z.; Yao, X.; Du, J.; Zhou, Z. Refined Evaluation of Satellite Precipitation Products against Rain Gauge Observations along the Sichuan–Tibet Railway. *J. Meteorol. Res.* **2022**, *36*, 779–797. <https://doi.org/10.1007/s13351-022-1226-z>.

Disclaimer/Publisher's Note: The statements, opinions and data contained in all publications are solely those of the individual author(s) and contributor(s) and not of MDPI and/or the editor(s). MDPI and/or the editor(s) disclaim responsibility for any injury to people or property resulting from any ideas, methods, instructions or products referred to in the content.